The Senescence-Associated-Secretory-Phenotype induced by centrosome amplification constitutes a pathway that activates Hypoxia-Inducible-Factor-α.

Selwin K. Wu[1,2,+]*, Juliana Ariffin[3], Remigio Picone[1,2]

[1]Department of Cell Biology, Harvard Medical School, Boston, MA, USA

[2]Department of Pediatric Oncology, Dana-Farber Cancer Institute, Boston, MA, USA

[3]Department of Surgery, Cancer Research Institute, Beth Israel Deaconess Medical Center, Harvard Medical School, Boston, MA, USA

[+]Present address: Mechanobiology Institute & Department of Biological Sciences, National University of Singapore

*Correspondence: selwin_wu@uqconnect.edu.au

ABSTRACT

The Senescence-Associated-Secretory Phenotype (SASP) can generate complex phenotypic outcomes by promoting tumor invasion in some contexts, but attracting cytotoxic T-cells and promoting the immune clearance of senescent cells in others. Here, we demonstrate that the SASP activated by centrosome amplification constitutes a pathway that activates hypoxia-inducible factor 1α and can trigger paracrine invasion. The SASP induced by centrosome amplification lacks detectable DNA damage or prominent NF-κB activation. Instead, the centrosome amplification induced SASP constitutes a pathway involving the activation of the small GTPase, Rac, the production of reactive oxygen species, the stabilization of the hypoxia-inducible factor 1α, and the consequent induction of prometastatic secreted factors such as ANGPTL4. We speculate that the commonly observed varied consequences of the SASP and the poor fitness of senescent cells may help explain why centrosome amplification promotes cancer-associated features in some experimental models but is neutral in others.

INTRODUCTION

Centrosomes promote the assembly and organization of microtubules, which in turn supports many cellular processes such as cell division, adhesion[1] and migration[2]. In most normal cells, centrosomes are duplicated once during each cell division such that G1 phase cells typically have one centrosome and mitotic cells have two. By contrast, cancer cells commonly exhibit increased numbers of centrosomes, termed centrosome amplification, which correlates with advanced tumour grade[3, 4] and promotes

spontaneous tumourigenesis in mice models when p53 is either deleted or becomes suppressed[5, 6].

Centrosome amplification promotes cellular invasion[7], mimicking the effects of oncogene activation. The underlying mechanism for cellular invasion is cell-autonomous, which involves activation of the small GTPase Rac by increased microtubules nucleation from extra centrosomes. Importantly, the presence of supernumerary centrosomes is deleterious to cells. Cells with extra centrosomes can undergo multipolar mitosis which leads to apoptosis or senescence[8]. Centrosome amplification also activates signaling pathways that promote p53 stabilization leading to cellular arrest[9]. Given these deleterious effects of centrosome amplification, it is surprising that most tumours maintain a subset of cells with extra centrosomes which are not outcompeted during tumour evolution. Thus, carrying the implication that a subset of cells with extra centrosomes may still provide an advantage to tumourigenesis. Recent work revealed that a minor subclone of cells overexpressing an interleukin can act as a dominant driver of tumourigenesis, by exerting paracrine effects on the extracellular matrix and surrounding cells[10, 11]. Here we find that centrosome amplification activates a Senescence-Associated-Secretory-Phenotype (SASP) that constitutes HIF1-α activation. The SASP functions through the action of its secreted factors independent of p53[12] and is well established to generate diverse phenotypic outcomes: promoting tumor invasion in some contexts[13-16], but attracting cytotoxic T-cells and promoting the immune clearance of senescent cells in others[17, 18]. The senescence program is variably characterized by several non-exclusive markers, including constitutive DNA damage response signalling, senescence-associated β-galactosidase (SA-βgal) activity, increased expression of the cyclin-dependent kinase (CDK) inhibitor p21CIP1 (CDKN1A) and increased secretion of many extracellular factors through the SASP program[19]. Many senescence-associated markers result from altered transcription, but the senescent phenotype is variable. This variability is attributed to tissue and cell-type differences, differences in the senescence trigger[19] and the dynamic nature of gene expression in senescent cells[20-22]. Despite variabilities in the senescent phenotype, a conserved transcriptome signature has recently been identified as a useful marker to consistently identify senescent cells[23]. Here we have identified a pathway for the centrosome amplification induced SASP to activate HIF1-α in epithelial cells.

RESULTS

Centrosome amplification induced a senescence-associated secretory phenotype (SASP).

Supernumerary centrosomes were generated in cells by overexpressing Polo-like kinase 4 (PLK4), the master regulatory kinase for centrosome duplication [24, 25]. PLK4 was induced transiently, and subsequent analysis was performed at time points where increased PLK4 mRNA was no longer detectable[7]. The

majority of MCF10A cells (approximately 80%) contains extra centrosomes after 48 hours of PLK4 induction (Supplementary Fig. 1a,b). In most experiments described below, transient overexpression of a truncated PLK4 mutant (Control 608) that has kinase activity but does not localize to the centrosomes[26] was used as the negative control.

To determine whether cells with centrosome amplification could induce paracrine invasion by tumor cells, using an established invasion assay with matrigel coated transwell[27]. MCF10A cells with or without centrosome amplification were introduced into the bottom chamber of transwells, which were separated from the top chamber by a matrigel insert. Invasion of MDA-MB468 cancer cells across the matrigel and filter barrier (Fig. 1a) was then measured. Strikingly, centrosome amplification induced an ~2.5-fold increase in invading MDA-MB468 relative to the controls lacking centrosome amplification (Fig. 1a,b,c). Thus, soluble factors from cells with centrosome amplification can induce cell motility and invasion of nearby cells.

Next, we used RNA sequencing to identify secreted factors induced by centrosome amplification. Transient PLK4 induction was used to induce centrosome amplification in MCF10A cells and RPE-1 cells, resulting in ~86% and ~91% of cells respectively with centrosome amplification (Supplementary Fig.1a, b). Seven days post-induction, the transcriptomes of cells with (PLK4) or without (Control 608) centrosome amplification were compared. Among 1987 genes with significantly altered expression in MCF10A cells (fold change (FC) $\geq \pm 2$, q-value < 0.05), 1285 were upregulated after centrosome amplification. For RPE-1 cells, 49 genes were significantly upregulated in cells with extra centrosomes. In both cell types after centrosome amplification, Ingenuity Pathway Analysis (IPA) revealed that the differentially expressed genes (fold change $\geq \pm 2$, q-value <0.05) were enriched for terms associated with inflammation and the senescence-associated secretory phenotype (SASP)[28-30] (Fig. 1d, Supplementary Fig. 1c). Importantly, the SASP can promote cell invasion[31].

Next, we queried the transcriptomes of cells with (PLK4) or without (Control 608) centrosome amplification for gene expression signatures of senescence and extracellular protein induction. Despite variabilities in the senescent phenotype, a core transcriptome signature, comprising of upregulated and downregulated genes have recently been identified as a useful marker to consistently identify senescent cells[23]. Thus, we employ this core senescent gene set to confirm the senescent identity of the whole-transcriptome-datasets analyzed here. Gene set enrichment analysis (GSEA)[32] in both MCF10A and RPE-1 cells revealed a strong association between centrosome amplification and senescence (FDR q=0.004, Fig 1e, FDR q=0.008, 1f, FDR q<0.001, 1g, FDR q=0.003, 1h) and extracellular region proteins(FDR

q<0.001, Fig. 1i, FDR q<0.001, 1j). The top 50 genes in the "extracellular region" GSEA leading-edge subset from both cell types contain a wide variety of secreted factors, including extracellular matrix proteins, angiogenic factors, cytokines, and pro-invasive factors including the SASP factor IL8 (Supplementary Fig 1d,e,).

We examine the effects of centrosome amplification with a PLK4 expression-independent approach by comparing the transcriptomes of newly-generated tetraploid cells from dicytochalasin B induced cytokinesis failure with doubled centrosome content to the parental diploid cells, as well as comparison with "evolved" tetraploid cells that had spontaneously lost their extra centrosomes [9, 33]. By IPA or GSEA with both data sets, the upregulated genes in newly generated tetraploids were enriched for secreted extracellular region proteins (FDR q<0.001, Supplementary Fig 1f,g), inflammatory and senescence-associated pathway terms (FDR q<0.001, Fig 1k,l and Supplementary Fig. 1h-k), in common with what we observed after senescence induced in MCF10A cells with 12Gy of γ-irradiation (Supplementary Fig. 1l). Thus, orthogonal experimental approaches suggest that centrosome amplification induces senescence and a senescence-associated secretome. Importantly, cytokinesis failure induces senescence[34]. Intriguingly, our data show that the spontaneous loss of extra centrosomes in tetraploids generated by cytokinesis failure is sufficient to down-regulate senescence-related gene expression changes.

Senescence is a complex and multifaceted phenomenon with no single cellular feature being sufficient to unambiguously identify cells as being "senescent". Under current convention, cells are typically defined as being senescent if they display proliferation arrest and at least two canonical senescence features[35, 36]. In addition to proliferation arrest (Fig 1m,n) and the SASP-like gene expression pattern, centrosome amplification induced other features of senescence. Consistent with a p53-dependent proliferation block, retinoblastoma phosphorylation was increased in cells with centrosome amplification (Fig. 1o). Also consistent with entry into senescence[37], centrosome amplification induced increased cell size as assayed by measurement of the volume of cells in suspension following trypsinization (~2 fold increase, Fig. 1p) or by measurement of adherent cell area (~2.4 fold increase, Fig. 1q). The induction of senescence-associated beta-galactosidase activity (~60% positive cells, Fig. 1r,s) was also observed in cells with extra centrosomes, albeit at a lower intensity and frequency than was observed after extensive DNA damage. Persistent DNA damage response leading to DNA damage foci marked by γH2AX, 53BP1, or ATM (Ataxia-Telangiectasia Mutated)[38, 39] is required for a robust SASP. However, multiple studies demonstrate that centrosome amplification does not induce detectable DNA damage in the primary nucleus[6, 9, 40]. Strikingly, even after ~8 days after the induction of extra centrosomes, when many features of senescence are obvious, we observed no significant increase in the percentage of γH2AX-positive cells

in the primary nucleus (Fig. 1t,u). Therefore, we reasoned that the weaker senescence detected by senescence-associated beta-galactosidase activity is due to a lack of extensive persistent DNA damage which is essential for a robust senescence phenotype.

Centrosome amplification promotes induction of ANGPTL4.

We next sought to identify secreted factors for paracrine invasion common to all conditions, including cytokinesis failure, where centrosome amplification was induced. From our gene expression profiles in different cell lines, 7 genes were strongly upregulated in all experimental conditions (Fig 2a, Supplementary Fig 2a and Supplementary Table 1). These included the cyclin-dependent kinase inhibitor p21 (Supplementary Fig 2b), which is induced in all known examples of senescence, and IGFBP3, a known inducer of senescence[41](Fig 2a,b). Among all conditions and cell types, ANGPTL4 was the most strikingly induced gene after centrosome amplification (up to ~15-fold induction in MCF10A cells, $p<0.001$ and approximately 5-fold in RPE-1 cells, Fig 2b,c). The induction of ANGPTL4 protein was confirmed using an enzyme-linked immunosorbent assay (ELISA) (Fig 2d). Importantly, inhibition of ANGPTL4 with a blocking-antibody or by CRISPR-mediated gene disruption significantly reduced paracrine invasion stimulated by MCF10A cells with extra centrosomes (Fig 2e,f and Supplementary Fig 2c-f). These findings are notable because ANGPTL4 is a well-established pro-invasive factor that activates Rac signalling, disrupts cell-cell contacts[42-45]. As expected, the increase expression of ANGPTL4 is a common feature of SASP[46].

Centrosome amplification activates HIF-1α induction of ANGPTL4.

We next addressed the mechanism by which centrosome amplification induces the expression of ANGPTL4. We considered the possibility that HIF-1α, the master regulator of the hypoxia response, is activated in the centrosome amplification induced SASP, because ANGPTL4 is an established HIF1α target[45, 47, 48]. HIFα are key transcription factors which regulate oxygen sensing and mediate the hypoxic response[49]. Activation of HIFα triggers the transcription of genes crucially involved in cancer[50] and immunity[51], including cytokines such as IL8, IL6, ANGPTL4, VEGF and PDGF which are commonly observed in SASP[31, 45, 52-54]. Consistent with this idea, GSEA demonstrated that a hallmark hypoxia gene signature is present in both MCF10A and RPE-1 cells with PLK4-induced centrosome amplification (FDR $q=0.028$, Figure 3a and FDR $q<0.001$, Supplementary Fig 2g). Additionally, newly generated tetraploid RPE-1 cells with extra centrosomes also exhibited enrichment of the hypoxia signature as compared with parental diploid cells (FDR $q=0.010$, Fig 3b) or evolved tetraploids lacking extra

centrosomes (FDR q<0.001, Fig 3c). To rigorously define a relevant hypoxia gene set in MCF10A cells, we derived a gene-expression signature of HIF α activation from transcriptomic analysis of MCF10A cells treated with Dimethyloxalylglycine, N- (Methoxyoxoacetyl)-glycine methyl ester (DMOG). DMOG promotes the steady-state accumulation of HIF-1 α by inhibiting EGLN/PHD prolyl hydroxlases[55]. Strikingly, this HIFα activation gene set was significantly enriched in both MCF10A and RPE-1 cells after centrosome amplification (FDR q<0.001, Fig 3d and FDR q=0.048, Supplementary Fig. 2h). By contrast, a previously reported data set for aneuploidy-induced senescence in RPE-1 cells[17] indicated that both the hallmark hypoxia gene set (FDR q=0.002, Fig 3e) and our DMOG-induced gene set (FDR q<0.001, Fig 3f) were suppressed in aneuploid cells, underscoring differences between the effects of centrosome amplification and aneuploidy[7].

Consistent with these gene expression results, using a HIF-1α specific antibody (Supplementary Fig 2i-k) we find that MCF-10A and RPE-1 cells with extra centrosomes exhibited a marked increase in nuclear HIF-1α (Fig. 3g,h,i Supplementary Fig 3l,m). HIF-1α accumulation was post-transcriptional because centrosome amplification did not affect HIF1α mRNA levels (Fig 3j). Moreover, centrosome amplification did not affect on the expression of proteins involved in HIF1α destruction (Fig. 3j). Importantly, CRISPR-mediated gene disruption of HIF-1α in cells with centrosome amplification blocked the activation of HIF α -regulated genes (FDR q=0.014, Supplementary Fig 2n,o), attenuated the induction of ANGPTL4 (Fig 3k), and reduced the capacity of these cells to promote paracrine invasion (Fig 3l and Supplementary Fig 2p). A total of 33 genes induced by centrosome amplification were critically dependent on HIF-1 α , including well established HIF-1 α targets such as VEGFA, VEGFC, ANGPTL4, LOXL2, and IL8 (Fig 3m and Supplementary Table 1). Among these, IL8 is an important cytokine that is known to be regulated by HIF-1α[56]. Accordingly, HIF1α disruption in cells with centrosome amplification reduced IL8 induction (Fig 3n).

The induction of HIF1α by centrosome amplification occurred regardless of whether cells were cultured in ambient oxygen tension (21% O_2) or under conditions of physiological normoxia/atmospheric hypoxia (5 % O_2). Gene expression profiles of RPE-1 cells with or without centrosome amplification were obtained after ~7 days in culture in 5% O_2. Consistent with our previous results obtained in ambient oxygen, cells in 5% oxygen with centrosome amplification exhibited strong upregulation of gene sets annotated for "extracellular proteins" (FDR q<0.001, Supplementary Fig. 3a), "senescence" (FDR q<0.001, FDR q=0.035, Supplementary Fig. 3b,c,) "hypoxia" and "HIF α activation"(FDR q<0.001, FDR q=0.004, Supplementary Fig 3d,e). Moreover, in physiological normoxia, we observed an enlarged

adherent cell size, an ~ 5 fold increase of nuclear HIF1 α (Supplementary Fig 3f,g), and induction of ANGPTL4 and p21 expression after centrosome amplification (Supplementary Fig 3h).

The activation of HIF1α that we have identified here is a non-canonical contributor of the SASP secretome. Instead, NF-κB is generally thought to be the primary determinant of the SASP secretome[39], and DNA damage signalling was recently shown to activate NF-κB through the transcription factor GATA4[38, 39]. However, centrosome amplification does not induce obvious DNA damage (Fig. 1p,q). Thus, quantitative imaging indicated that centrosome amplification in three cell lines did not result in any detectable increase in the nuclear localization of NF-κB (Fig. 3o-q and Supplementary Fig. 3i). Because secreted factors regulated by NFκB reinforce senescence[39], poor NFκB activation likely contributes to the weaker induction of senescence-associated beta-galactosidase activity by centrosome amplification (Fig 1 n,o). Although, evidence suggests that hypoxia and HIFα activation can prevent or delay cells from entering senescence[57]. Nevertheless, the HIFα activity of cells once they have entered senescence have not been studied. Our data show that centrosome amplification induced SASP constitutes activation of HIF α .

Centrosome amplification activates HIF-1 α through induction of ROS.

ROS is induced by inflammatory cytokines, a common feature of senescence and an established trigger for HIF-1 α activation[55, 58]. Therefore, we considered the possibility that increased levels of reactive oxygen species (ROS) could provide a mechanistic link between centrosome amplification and HIF1 α activation. We previously reported that centrosome amplification activates the Rho-type GTPase Rac1[7]. Among its many functions, Rac promotes ROS production because it is a stoichiometric subunit of the NADPH oxidase[42, 59]. Therefore, we tested the hypothesis that after centrosome amplification, the Rac -NADPH oxidase generates ROS, which activates HIF1α. Consistent with this hypothesis, pharmacological inhibition of Rac (Fig 4a and Supplementary Fig 4a), CRISPR-mediated gene disruption of the Rac GTPase exchange factor, Trio[60, 61] (Fig 4b, c and Supplementary Fig 4b,c), or siRNA knockdown of a key component of the NADPH oxidase, $p22^{phox}$, (Fig 4d and Supplementary Fig 4d,e,f) all significantly reduced HIF-1 α nuclear accumulation in cells with centrosome amplification. By RNA sequencing, CRISPR-mediated gene disruption of Trio also suppressed gene expression signatures associated with HIF α activation, including the induction of ANGPTL4, without significantly affecting HIF α regulated genes in control cells (FDR q=0.0294, Fig 4e, f and FDR q=0.044, Supplementary Fig 4g,h).

Centrosome amplification induces Rac activation[7, 62]. When Rac is activated, NADPH oxidase complex can generate superoxide[63]. Using dihydroethidium labelling, we found that cells with centrosome amplification indeed exhibit higher levels of superoxide (Fig 4g and Supplementary Fig 5a). Cells convert superoxide into the more stable hydrogen peroxide by dismutation of superoxide[64]. Both cellular superoxide and hydrogen peroxide promote HIF1α stabilization[58, 65]. However, when we accelerated the conversion of superoxide into hydrogen peroxide by treatment of cells with TEMPOL[65], nuclear HIF1α levels are further increased (Fig 4h and Supplementary Fig 5b), suggesting that that hydrogen peroxide is the dominant ROS species inducing HIF-1α stabilization after centrosome amplification. Next, we used catalase addition to the culture medium to directly deplete hydrogen peroxide[66]. Strikingly, in cells with centrosome amplification, catalase treatment prevented nuclear HIF-1α accumulation and suppressed the HIF α -associated gene expression, including the transcriptional induction of ANGPTL4 (Fig 4f,i,j, FDR q=0.009, 4k, and Supplementary Fig 5c). Thus, suggesting that the Rac-NADPH oxidase complex generated ROS activates HIF1α in cells with extra centrosomes. Although ROS induction of HIFα is a prominent feature of the SASP from centrosome amplification, elevated ROS is observed in many forms of senescence[37].

The hypoxia signalling may not be specific to centrosome amplification induced SASP. Indeed, consistent with previous evidence that gamma irradiation activates HIF-1α[67], nuclear HIF-1α accumulates in γ-irradiation induced senescent cells and we observed enrichment of hypoxia-induced genes and a HIFα activation signature (Supplementary Fig 5d-g). HIF-1α is also known to be activated by Ras signaling[68]. Accordingly, we observed enrichment of hypoxia-induced genes and a HIFα activation signature in published data sets[69] where senescence is induced by oncogene activation (FDR q<0.001, Supplementary Fig 5h,i) Although, the senescence phenotype exhibits significant variability across different cell lines and with different approaches to induces senescence. Our data show that the expression of hypoxia-induced genes could still be detected in other forms of senescence as well.

In summary, our findings demonstrate that centrosome amplification promotes a senescence-associated secretory phenotype (SASP) that constitutes of HIF1α activation in cultured cells (Supplementary Fig 5j). The SASP is well established to generate diverse phenotypic outcomes: promoting tumor invasion in some contexts[13-16], but attracting cytotoxic T-cells and promoting the immune clearance of senescent cells in others[17, 18]. We speculate that the varied consequences of senescence may help explain why centrosome amplification promotes tumourigenesis in some mice models[6, 7] but is neutral in others[70, 71].

Acknowledgements

We gratefully thank I. Ghobrial, S. Papathanasiou, A. Spektor, A.J. Holland, W. Johnson, Y. Kaplan, H. Zhang, A. Yap, S. Liu, K. Briggs, H. Nicholson, W. Kaelin, S.Godinho and K. Polyak for their unstinting support and advice during this project. A.Spektor for gamma irradiation experiments, L. Hodgson, M. Janiszewska and H. Zhang for technical advice and reagents, F. Abderazza, N. Flanagan, Y. Wang, D. Deconti, and B. Lawney from the Centre for Cancer Computational Biology and X. Qiu and H. Long from Center for Functional Cancer Epigenetics for help with bioinformatics analysis. SKW was supported by a Leukemia and Lymphoma Society Fellow Award (5454-17) and on a Research Scholarship Block Research Fellow Scheme by the Ministry of Education, Singapore. RP was supported by a Susan G. Komen Postdoctoral Fellowship (PDF15333560). We acknowledge the Nikon Imaging Center at Harvard Medical School for imaging support.

FIGURE LEGENDS

Figure 1. Centrosome amplification triggers a senescence-associated secretory phenotype (SASP) independent of DNA damage.

(a) Experimental scheme for the matrigel coated transwell invasion experiment. Transwell inserts physically separates mCherry MDA-MB468 cells (top chamber) from the indicated MCF10A cells (bottom chamber). Paracrine invasion is scored from the numbers of mCherry MDA-MB468 cells that migrate to the bottom chamber.

(b,c) MCF10A cells with centrosome amplification promote the invasion of MDA-MB468 mCherry cells. Representative images (b) and fold increase (c) of mCherry MDA-MB468 cells that crossed the matrigel coated transwell upon co-cultured with the indicated MCF10A cells. All data are means + s.e.m. from n=3 independent experiments, ns, not significant; *$P < 0.05$, analysed with one-way ANOVA, Tukey's multiple comparison test. Scale bars, 50 μm.

(d) Centrosome amplification alters expression of genes related to cell motility and senescence. Ingenuity Pathway Analysis (IPA) of gene expression changes in MCF10A cells with centrosome amplification relative to controls revealing the top pathways altered by centrosome amplification.

(e-h) Induction of senescence-related genes expression in cells with centrosome amplification. Gene set enrichment analysis (GSEA) revealed strong enrichment of genes up-regulated (e,g) or down-regulated (f,h) with senescence in MCF10A cells with centrosome amplification (e,f) and tetraploid RPE-1 cells (g,h) relative to controls. NES: normalized enrichment score; FDR: false discovery rate.

(i,j) Proliferation arrest after centrosome amplification. Representative images (i) and quantification (j) of cells that cycled through S-phase (24 hr. EdU-label, red) and DAPI (blue) in MCF10A cells with (PLK4) and without (608) centrosome amplification.

(k) Centrosome amplification induces retinoblastoma protein phosphorylation. Rb, Phospho Rb S780 and GAPDH (loading control) immunoblots of lysates from MCF10A cells with and without centrosome amplification.

(l,m) Centrosome amplification increases cell size. Suspended (trypsinized) (j) and adherent (k) cell size measured for MCF10A cells with or without centrosome amplification.

(n,o) Increased SA- β -Gal staining in cells with centrosome amplification. Representative images (n) and quantification (o) of SA- β -Gal (blue) staining of MCF10A cells with and without centrosome amplification or positive control with doxorubicin treatment.

(p,q) Centrosome amplification does not induce DNA-damage. Representative images (p) and quantification (q) of γH2AX foci (green) in MCF10A cells with (PLK4) and without (608) centrosome amplification as compared to DNA damage from doxorubicin treatment. Cells in S-phase are labelled with Edu(red) pulse and excluded from the quantification. All data are means $\pm$ s.e.m. from n=3 independent experiments,**P < 0.01,****P <0.0001; analysed with Student's t–test except **m** which was with one-way ANOVA, Tukey's multiple comparison test. Scale bars, 50 μ m.

Figure 2. Centrosome amplification induced ANGPTL4.

(a) Seven genes are upregulated by centrosome amplification from all experimental conditions, in two cell types. Venn diagram for the indicated comparisons showing the overlap of upregulated genes from RNAseq (2 fold change, p(adjusted)<0.05).

(b) Among the 7 commonly upregulated genes, ANGPTL4 expression is the most strongly induced by centrosome amplification. Fold induction for this group of genes from RNAseq of MCF10A cells with centrosome amplification relative to controls.

(c) Induction of ANGPTL4 expression in cells with centrosome amplification. ANGPTL4 mRNA fold changes from RNAseq in RPE-1 cells in PLK4 versus 608, tetraploids versus parental diploids and tetraploids versus evolved tetraploids.

(d) Induction of ANGPTL4 secretion in cells with centrosome amplification. ELISA analysis of secreted ANGPTL4 from cells with or without centrosome amplification.

(e) Inhibition of ANGPTL4 compromises paracrine invasion stimulated by cells with centrosome amplification. Shown is the fold increase of MDA-MB468 cells in the bottom chamber of the transwell in the presence of either control IgG or an ANGPTL4 blocking antibody, co-cultured with the indicated MCF10A cells.

(f) CRISPR-mediated gene disruption of ANGPTL4 in cells with centrosome amplification inhibits induction of paracrine invasion. Fold increase of MDA-MB468 cells that crossed the Matrigel coated transwell filter upon co-cultured with control or sgANGPTL4 MCF10A cells with centrosome amplification.

All data are means $\pm$ s.e.m. from n=3 independent experiments, *P < 0.05; analysed with Student's t -test. **P <0.01, ****P <0.0001 ; adjusted P value (grey) analysed with DESeq2 Wald test.

Figure 3. Centrosome amplification activates HIF1α.

(a-c) Induction of the expression of hypoxia-inducible genes in cells with centrosome amplification. GSEA revealed a strong enrichment of an annotated hypoxia hallmark gene set in cells with centrosome amplification. RNA-seq data sets being compared are indicated at the bottom of the GSEA plots for MCF10A cells (a) and RPE-1 cells (b & c).

(d) A custom-generated HIFα signature up gene set in MCF10A cells is strongly induced by centrosome amplification in MCF10A cells.

(e,f) Unlike centrosome amplification, aneuploidy-induced senescence suppresses expression of the hallmark hypoxia (e) and custom-generated MCF10A HIFα signature up (f) gene sets.

(g-i) Induction of nuclear HIF-1α after centrosome amplification-induced senescence. Representative images (g) and automated quantification of nuclear HIF-1α in MCF10A cells (h) or RPE-1 cells (i) with or without centrosome amplification (see online Methods and Supplementary Fig 4).

(j) Centrosome amplification does not alter the expression of HIF-1α, VHL and EGLN1. Fold difference of HIF-1α, VHL and EGLN1 expression levels from MCF10A cells RNA-seq data sets with or without

centrosome amplification.

(k) CRISPR-mediated gene disruption of HIF-1 α reduces ANGPTL4 expression induced by centrosome amplification. The relative abundance of ANGPTL4 mRNA from RNAseq in centrosome amplification or control hypoxia mimetic DMOG-treated cells is expressed as the fold-change with respect to control cells. Centrosome amplification and control 608 cells are subjected to CRISPR-mediated gene disruption of HIF-1α and compared to CRISPR non-targeting sgRNA controls.

(l) CRISPR-mediated gene disruption of HIF-1 α in cells with centrosome amplification inhibits the induction of paracrine invasion. Fold increase of MDA-MB468 cells that invaded across the matrigel coated transwell when co-cultured with control or sgHIF1α MCF10A cells with centrosome amplification.

(m) Forty-nine genes are significantly induced by centrosome amplification induced HIF-1α activation. Venn diagram for the indicated comparisons showing the overlap of the leading-edge subsets of genes from GSEA of HIF α -induced genes.

(n) CRISPR-mediated gene disruption of HIF-1 α reduces IL8 expression induced by centrosome amplification. Relative abundance of IL8 mRNA from RNAseq in centrosome amplification or DMOG-treated cells is expressed as the fold change relative to controls. Centrosome amplification and control cells are subjected to CRISPR-mediated gene disruption of HIF-1 α and compared to the CRISPR non-targeting control.

(o) Lack of NF-κB nuclear accumulation after centrosome amplification. Representative images of p65 RELA (NF-κB) and DAPI (grey) in MCF10A cells with and without centrosome amplification as compared with a K-RasG12V positive control.

(p,q) Quantification of p65 RELA (NF-κB) nuclear/cytoplasmic ratio in MCF10-A (p) and RPE-1 (q) cells with or without centrosome amplification as compared to K-RasG12V overexpression (p) or TNFα treatment (q).

All data are means $\pm$ s.e.m. from n=3 independent experiments, **P < 0.01, ***P < 0.001,****P <0.0001; analysed with one-way ANOVA, Tukey's multiple comparison test.. Scale bars, 50 μ m.

Figure 4. Centrosome amplification induced ROS.

(a) Small molecule Rac-1 inhibition prevents the accumulation of nuclear HIF-1α after centrosome amplification. The indicated MCF10A cells were treated with 50μm NSC23766 or vehicle and HIF-1α nuclear accumulation was measured.

(b,c) CRISPR-mediated gene disruption of TRIO blocks nuclear HIF-1α accumulation after centrosome amplification. Gene targeting of a pool of cells was performed in the indicated MCF10A cells prior to the initiation of centrosome amplification. Shown are representative image (b) and quantification (c) of nuclear HIF1α levels in the indicated cells.

(d) siRNA knockdown of $p22^{phox}$ inhibits nuclear HIF-1α accumulation after centrosome amplification as in (c).

(e) Trio is required for the upregulation of HIFα-induced genes in MCF10A cells with centrosome amplification. Shown is a GSEA plot comparing cells with centrosome amplification with or without TRIO gene disruption.

(f) The induction of ANGPTL4 by centrosome amplification requires Trio and ROS. Shown is the fold-induction of ANGPTL4 from RNAseq after centrosome amplification in MCF10A cells after the indicated treatments.

(g) Accumulation of superoxide after centrosome amplification Superoxide levels were measured by dihydroethidium-labelling in MCF10A cells with and without centrosome amplification. Pyocyanin treatment is the positive control.

(h) Conversion of superoxide into hydrogen peroxide further induces nuclear HIF-1α accumulation in cells with centrosome amplification. Shown are the fold changes in nuclear HIF-1α in the indicated MCF10A cells after treatment with TEMPOL.

(i,j) Catalase blocks the nuclear accumulation of HIF-1α in cells with centrosome amplification. Representative images (i) and quantification (j) of HIF1α in the indicated MCF10A cells with and without catalase medium addition.

(k) GSEA showing that catalase treatment prevents the upregulation of the custom HIFα signature up gene set in MCF10A cells. All data are means ± s.e.m. from n=3 independent experiments, *P < 0.05, **P < 0:01, ***P < 0:001,****P <0:0001; analysed with one-way ANOVA, Tukey's multiple comparison

test.Scale bars, 50 μ m.

SUPPLEMENTARY FIGURE LEGENDS

Supplementary Figure 1. Features of the centrosome amplification SASP.

(a,b) The fraction of control (608) and PLK4 induced MCF10A(a) or RPE-1(b) cells with more than 2 centrosomes determined by immunostaining of centrin-1. Data are means ± s.e.m. from n=2 independent experiments.

(c) Centrosome amplification alters expression of genes related to cell motility and senescence. Ingenuity Pathway Analysis (IPA) of gene expression changes in RPE-1 cells with centrosome amplification relative to controls revealing the top pathways altered by centrosome amplification.

(d,e) Induction of secreted protein expression in cells with centrosome amplification. Gene set enrichment analysis (GSEA) revealed enrichment of genes annotated to be the extracellular region in tetraploids relative to either parental diploids (d) or evolved tetraploids (e). NES: normalized enrichment score; FDR: false discovery rate.

(f,g) Induction of the expression of secreted proteins in cells with centrosome amplification. Heatmap showing the leading-edge enrichment of the top 50 extracellular protein expression upregulated in MCF10A (f) and RPE-1 (g) cells with centrosome amplification relative to control.

(h,i) Centrosome amplification alters expression of genes related to senescence. Ingenuity Pathway Analysis (IPA) of gene expression changes in tetraploids relative to either parental diploids (h) or evolved tetraploids (i) revealing the top pathways altered by centrosome amplification.

(j,k) Heatmap showing the leading-edge enrichment of the top 50 extracellular protein expression upregulated in tetraploids relative to either parental diploids (i) or evolved tetraploids (j).

(l) γ-irradiation alters expression of genes related to DNA-damage induced senescence. Ingenuity Pathway Analysis (IPA) of gene expression changes in MCF10A cells exposed to 12Gy of γ-irradiation relative to controls revealing the top pathways altered by DNA-damage induced senescence.

Supplementary Figure 2. Gene expression altered by centrosome amplification, a functional requirement for ANGPTL4

(a) Zero genes are commonly downregulated by centrosome amplification from all experimental conditions. Venn diagram for the indicated comparisons showing the overlap of downregulated genes

from RNAseq (2 fold change, q<0.05).

(b) Induction of p21 expression in cells with centrosome amplification. p21 mRNA fold changes from RNAseq in RPE-1 and MCF10A cells in PLK4 versus 608, tetraploids versus parental diploids and tetraploids versus evolved tetraploids. Data are means ± s.e.m. from n=3 independent experiments, ****P <0:0001; adjusted P-value(grey) analysed with DESeq2 Wald test.

(c) CRISPR-mediated gene disruption of ANGPTL4. ANGPTL4 and GAPDH (loading control) immunoblots of lysates from doxycycline uninduced control PLK4, sgANGPTL4 PLK4, control 608 and sgANGPTL4 608 cells.

(d) CRISPR-mediated gene disruption of ANGPTL4 does not affect the induction of extra centrosomes. The fraction of control (608) and PLK4 induced sgANGPTL4 MCF10A cells with more than 2 centrosomes, determined by immunostaining of centrin-1. Data are means ± s.e.m. from n=2 independent experiments.

(e) Inhibition of ANGPTL4 compromises paracrine invasion stimulated by cells with centrosome amplification. Shown is the representative image of MDA-MB468 cells in the bottom chamber of the transwell in the presence of either control IgG or an ANGPTL4 blocking antibody, co-cultured with the indicated MCF10A cells.

(f) CRISPR-mediated gene disruption of ANGPTL4 in cells with centrosome amplification inhibits paracrine invasion. Shown is the representative image of MDA-MB468 cells that crossed the Matrigel-coated transwell upon co-culturing with control or sgANGPTL4 MCF10A cells with centrosome amplification. Scale bars, 50 μm.

(g,h) Centrosome amplification upregulates the expression of hypoxia and DMOG-induced genes. GSEA revealed strong enrichment of an annotated hypoxia hallmark gene set (g) and DMOG-induced genes (h) in cells with centrosome amplification. RNA-seq datasets being compared are indicated at the bottom of the GSEA plots for RPE-1 cells.

(i) The HIF-1α monoclonal antibody is specific. Representative images of HIF-1α in DMOG-treated, DMSO(vehicle) and DMOG-treated sgHIF-1α cells.

(j) HIF-1α cytoplasmic fluorescence intensity is largely background staining. Automated quantification of cytoplasmic mean fluorescence intensity of HIF-1α in DMOG-treated, DMSO(vehicle) and DMOG-treated sgHIF-1α cells. For Cont DMSO, n= 210; Cont DMOG, n=265; sgHIF-1α DMOG, n=464.

(k) DMOG induces nuclear HIF-1α. Automated quantification of nuclear HIF-1α above cytoplasmic levels in DMOG-treated, DMSO(vehicle) and DMOG-treated sgHIF-1α cells. For Cont DMSO, n= 210; Cont DMOG, n=265; sgHIF-1α DMOG, n=464.

(l) CRISPR-mediated gene disruption of HIF1A does not affect the induction of extra centrosomes. The fraction of control (608) and PLK4 induced sgHIF-1α MCF10A cells with more than 2 centrosomes, determined by immunostaining of centrin-1. Data are means ± s.e.m. from n=2 independent experiments.

(m) Induction of nuclear HIF-1α after centrosome amplification-induced senescence. Representative images of HIF-1α in RPE-1 cells with or without centrosome amplification.

(n) CRISPR-mediated gene disruption of HIF-1α. HIF-1α and GAPDH (loading control) immunoblots of lysates from doxycycline uninduced control PLK4, sgHIF1A PLK4, control 608 and sgHIF1A 608 cells which are DMOG-treated.

(o) The custom HIFα signature up gene set is specific for centrosome amplification induced HIF-1α activation. GSEA showing that CRISPR-mediated gene disruption suppresses the custom HIFα signature up gene set in sgHIF1A cells relative to control PLK4 MCF10A cells.

(p) CRISPR-mediated gene disruption of HIF1A in cells with centrosome amplification inhibits induction of paracrine invasion. Shown is the representative image of MDA-MB468 cells that crossed the matrigel coated transwell upon co-cultured with control or sgHIF1A MCF10A cells with centrosome amplification. Scale bars, 50 μm. All data are means ± s.e.m. from 2 independent experiments analysed with one-way ANOVA, Tukey's multiple comparison test. Scale bars, 50 μm.

Supplementary Figure 3. Centrosome amplification induced a SASP that constitutes HIF1α activation independent of prominent NF- κB activity.

(a-e) Induction of senescence-associated genes expression in cells with centrosome amplification cultured in physiological normoxia. By GSEA, RPE-1 cells with centrosome amplification cultured in 5% O_2 induce gene sets associated with the extracellular region(a), genes upregulated(b) and downregulated(c)

in senescence, hypoxia(d) and the custom HIFα signature gene set (e).

(f,g) Centrosome amplification induces nuclear HIF1α in RPE-1 cells when cells are cultured in 5% O_2. Representative images (f) and quantification (g) of nuclear HIF-1α in the indicated RPE-1 cells.

(h) Fold induction of ANGPTL4 and p21 from RNAseq of cells cultured in 5% O_2 relative to controls.

(i) Lack of NF- κB nuclear accumulation after centrosome amplification. Representative images of p65 RELA (NF- κB) and DAPI (grey) in RPE-1 with and without centrosome amplification as compared with a TNFα treatment positive control.

Supplementary Figure 4. A pathway linking centrosome amplification to HIF-1α activation

(a) Small molecule Rac inhibition prevents the accumulation of nuclear HIF-1α after centrosome amplification. Representative images of the indicated MCF10A cells were treated with 50 μ m NSC23766 or vehicle and HIF-1α nuclear accumulation was measured.

(b) CRISPR-mediated gene disruption of TRIO. Trio and GAPDH (loading control) immunoblots of lysates from doxycycline uninduced control PLK4, sgTrio PLK4, control 608 and sgTrio 608 cells.

(c) CRISPR-mediated gene disruption of Trio does not affect the induction of extra centrosomes. The fraction of control 608 and PLK4 induced sgTRIO MCF10A cells with more than 2 centrosomes, determined by immunostaining of centrin-1. Data are means $\pm$ s.e.m. from n=2 independent experiments.

(d) siRNA knockdown of $p22^{phox}$. $p22^{phox}$ and GAPDH (loading control) immunoblots of lysates from doxycycline uninduced control PLK4, $p22^{phox}$ knockdown PLK4, control 608 and $p22^{phox}$ knockdown 608 cells.

(e) siRNA knockdown of $p22^{phox}$ does not affect the induction of extra centrosomes. The fraction of control (608) and PLK4 induced $p22^{phox}$ knockdown MCF10A cells with more than 2 centrosomes, determined by immunostaining of centrin-1. Data are means $\pm$ s.e.m. from n=2 independent experiments.

(f) siRNA knockdown of $p22^{phox}$ prevents the accumulation of nuclear HIF-1α after centrosome amplification. Representative images of HIF-1α of the indicated MCF10A cells.

(g) TRIO is required for the upregulation of hypoxia-induced genes in MCF10A cells with centrosome amplification. Shown is a GSEA plot comparing cells with centrosome amplification

with or without TRIO gene disruption.

(h) CRISPR-mediated gene disruption of Trio does not significantly affect the regulation of HIF-1α and hypoxia-induced genes in MCF10A control 608 cells. Shown are the normalized enrichment score and false discovery rate q-values of HIF-1α and hypoxia-induced genes for sgTrio 608 cells relative to control 608 cells. Scale bars, 50 μm.

Supplementary Figure 5. The role of hydrogen peroxide in the activation of HIF-1α after centrosome amplification and activation of HIFα by gamma-irradiation and oncogene-induced senescence.

(a) Accumulation of superoxide after centrosome amplification. Representative images of dihydroethidium-labelling of superoxide levels in MCF10A cells with and without centrosome amplification. Pyocyanin treatment is the positive control.

(b) Conversion of superoxide into hydrogen peroxide further induces nuclear HIF1α accumulation in cells with centrosome amplification. Representative images of HIF-1α in the indicated MCF10A cells after treatment with TEMPOL.

(c) GSEA showing that catalase treatment prevents the upregulation of the hallmark hypoxia gene set in MCF10A cells.

(d,e) Nuclear HIF1α levels are significantly increased in senescent cells 8 days post γ-irradiation. Representative images (d) and quantification (e) of nuclear HIF1α (grey) in control and senescent MCF10A cells.

(f-i) GSEA showing that the hallmark hypoxia gene sets and custom HIFα signature up (HIFα) are upregulated in MCF10A cells 8 days post γ-irradiation (f,g) and IMR90 cells undergoing oncogene-induced senescence[69] (h,i).

Scale bars, 50 μm. Data are means ± s.e.m. from n=2 independent experiments, *P < 0.05; analysed with Student's t -test. Scale bar, 50 μm.

REFERENCES

1. Akhmanova, A., Stehbens, S.J. & Yap, A.S. Touch, grasp, deliver and control: functional cross-talk between microtubules and cell adhesions. *Traffic* **10**, 268-274 (2009).

2. Etienne-Manneville, S. Microtubules in cell migration. *Annu Rev Cell Dev Biol* **29**, 471-499 (2013).
3. Gonczy, P. Centrosomes and cancer: revisiting a long-standing relationship. *Nat Rev Cancer* **15**, 639-652 (2015).
4. Chan, J.Y. A clinical overview of centrosome amplification in human cancers. *Int J Biol Sci* **7**, 1122-1144 (2011).
5. Sercin, O. *et al.* Transient PLK4 overexpression accelerates tumorigenesis in p53-deficient epidermis. *Nat Cell Biol* **18**, 100-110 (2016).
6. Levine, M.S. *et al.* Centrosome Amplification Is Sufficient to Promote Spontaneous Tumorigenesis in Mammals. *Dev Cell* **40**, 313-322 e315 (2017).
7. Godinho, S.A. *et al.* Oncogene-like induction of cellular invasion from centrosome amplification. *Nature* **510**, 167-171 (2014).
8. Kwon, M. *et al.* Mechanisms to suppress multipolar divisions in cancer cells with extra centrosomes. *Genes Dev* **22**, 2189-2203 (2008).
9. Ganem, N.J. *et al.* Cytokinesis failure triggers hippo tumor suppressor pathway activation. *Cell* **158**, 833-848 (2014).
10. Marusyk, A. *et al.* Non-cell-autonomous driving of tumour growth supports sub-clonal heterogeneity. *Nature* **514**, 54-58 (2014).
11. Janiszewska, M. *et al.* Subclonal cooperation drives metastasis by modulating local and systemic immune microenvironments. *Nat Cell Biol* **21**, 879-888 (2019).
12. Coppe, J.P. *et al.* Senescence-associated secretory phenotypes reveal cell-nonautonomous functions of oncogenic RAS and the p53 tumor suppressor. *PLoS Biol* **6**, 2853-2868 (2008).
13. Angelini, P.D. *et al.* Constitutive HER2 signaling promotes breast cancer metastasis through cellular senescence. *Cancer Res* **73**, 450-458 (2013).
14. Kim, Y.H. *et al.* Senescent tumor cells lead the collective invasion in thyroid cancer. *Nat Commun* **8**, 15208 (2017).
15. Gluck, S. *et al.* Innate immune sensing of cytosolic chromatin fragments through cGAS promotes senescence. *Nat Cell Biol* **19**, 1061-1070 (2017).
16. Dou, Z. *et al.* Cytoplasmic chromatin triggers inflammation in senescence and cancer. *Nature* **550**, 402-406 (2017).
17. Santaguida, S. *et al.* Chromosome Mis-segregation Generates Cell-Cycle-Arrested Cells with Complex Karyotypes that Are Eliminated by the Immune System. *Dev Cell* **41**, 638-651 e635 (2017).
18. Eggert, T. *et al.* Distinct Functions of Senescence-Associated Immune Responses in Liver Tumor Surveillance and Tumor Progression. *Cancer Cell* **30**, 533-547 (2016).
19. Sharpless, N.E. & Sherr, C.J. Forging a signature of in vivo senescence. *Nat Rev Cancer* **15**, 397-408 (2015).
20. Hoare, M. *et al.* NOTCH1 mediates a switch between two distinct secretomes during senescence. *Nat Cell Biol* **18**, 979-992 (2016).
21. Lee, S. & Schmitt, C.A. The dynamic nature of senescence in cancer. *Nat Cell Biol* **21**, 94-101 (2019).
22. Schmitt, C.A. The persistent dynamic secrets of senescence. *Nat Cell Biol* **18**, 913-915 (2016).
23. Hernandez-Segura, A. *et al.* Unmasking Transcriptional Heterogeneity in Senescent Cells. *Curr Biol* **27**, 2652-2660 e2654 (2017).
24. Bettencourt-Dias, M. *et al.* SAK/PLK4 is required for centriole duplication and flagella development. *Curr Biol* **15**, 2199-2207 (2005).
25. Habedanck, R., Stierhof, Y.D., Wilkinson, C.J. & Nigg, E.A. The Polo kinase Plk4 functions in centriole duplication. *Nat Cell Biol* **7**, 1140-1146 (2005).

26. Guderian, G., Westendorf, J., Uldschmid, A. & Nigg, E.A. Plk4 trans-autophosphorylation regulates centriole number by controlling betaTrCP-mediated degradation. *J Cell Sci* **123**, 2163-2169 (2010).
27. Pan, M. *et al.* BNIP-2 retards breast cancer cell migration by coupling microtubule-mediated GEF-H1 and RhoA activation. *Sci Adv* **6**, eaaz1534 (2020).
28. Krizhanovsky, V. *et al.* Senescence of activated stellate cells limits liver fibrosis. *Cell* **134**, 657-667 (2008).
29. Jeon, O.H. *et al.* Local clearance of senescent cells attenuates the development of post-traumatic osteoarthritis and creates a pro-regenerative environment. *Nat Med* **23**, 775-781 (2017).
30. Childs, B.G. *et al.* Senescent intimal foam cells are deleterious at all stages of atherosclerosis. *Science* **354**, 472-477 (2016).
31. Coppe, J.P., Desprez, P.Y., Krtolica, A. & Campisi, J. The senescence-associated secretory phenotype: the dark side of tumor suppression. *Annu Rev Pathol* **5**, 99-118 (2010).
32. Subramanian, A. *et al.* Gene set enrichment analysis: a knowledge-based approach for interpreting genome-wide expression profiles. *Proc Natl Acad Sci U S A* **102**, 15545-15550 (2005).
33. Ganem, N.J., Godinho, S.A. & Pellman, D. A mechanism linking extra centrosomes to chromosomal instability. *Nature* **460**, 278-282 (2009).
34. Panopoulos, A. *et al.* Failure of cell cleavage induces senescence in tetraploid primary cells. *Mol Biol Cell* **25**, 3105-3118 (2014).
35. Perez-Mancera, P.A., Young, A.R. & Narita, M. Inside and out: the activities of senescence in cancer. *Nat Rev Cancer* **14**, 547-558 (2014).
36. Gorgoulis, V. *et al.* Cellular Senescence: Defining a Path Forward. *Cell* **179**, 813-827 (2019).
37. Kuilman, T., Michaloglou, C., Mooi, W.J. & Peeper, D.S. The essence of senescence. *Genes Dev* **24**, 2463-2479 (2010).
38. Rodier, F. *et al.* Persistent DNA damage signalling triggers senescence-associated inflammatory cytokine secretion. *Nat Cell Biol* **11**, 973-979 (2009).
39. Kang, C. *et al.* The DNA damage response induces inflammation and senescence by inhibiting autophagy of GATA4. *Science* **349**, aaa5612 (2015).
40. Holland, A.J., Fachinetti, D., Han, J.S. & Cleveland, D.W. Inducible, reversible system for the rapid and complete degradation of proteins in mammalian cells. *Proc Natl Acad Sci U S A* **109**, E3350-3357 (2012).
41. Kim, K.S. *et al.* Regulation of replicative senescence by insulin-like growth factor-binding protein 3 in human umbilical vein endothelial cells. *Aging Cell* **6**, 535-545 (2007).
42. Zhu, P. *et al.* Angiopoietin-like 4 protein elevates the prosurvival intracellular O2(-):H2O2 ratio and confers anoikis resistance to tumors. *Cancer Cell* **19**, 401-415 (2011).
43. Huang, R.L. *et al.* ANGPTL4 modulates vascular junction integrity by integrin signaling and disruption of intercellular VE-cadherin and claudin-5 clusters. *Blood* **118**, 3990-4002 (2011).
44. Padua, D. *et al.* TGFbeta primes breast tumors for lung metastasis seeding through angiopoietin-like 4. *Cell* **133**, 66-77 (2008).
45. Zhang, H. *et al.* HIF-1-dependent expression of angiopoietin-like 4 and L1CAM mediates vascular metastasis of hypoxic breast cancer cells to the lungs. *Oncogene* **31**, 1757-1770 (2012).
46. Zhang, B. *et al.* The senescence-associated secretory phenotype is potentiated by feedforward regulatory mechanisms involving Zscan4 and TAK1. *Nat Commun* **9**, 1723 (2018).

47. Li, H. *et al.* Hypoxia-inducible factor 1 alpha-activated angiopoietin-like protein 4 contributes to tumor metastasis via vascular cell adhesion molecule-1/integrin beta1 signaling in human hepatocellular carcinoma. *Hepatology* **54**, 910-919 (2011).
48. Semenza, G.L. Molecular mechanisms mediating metastasis of hypoxic breast cancer cells. *Trends Mol Med* **18**, 534-543 (2012).
49. Kietzmann, T., Mennerich, D. & Dimova, E.Y. Hypoxia-Inducible Factors (HIFs) and Phosphorylation: Impact on Stability, Localization, and Transactivity. *Front Cell Dev Biol* **4**, 11 (2016).
50. Miroshnikova, Y.A. *et al.* Tissue mechanics promote IDH1-dependent HIF1alpha-tenascin C feedback to regulate glioblastoma aggression. *Nat Cell Biol* **18**, 1336-1345 (2016).
51. Palazon, A., Goldrath, A.W., Nizet, V. & Johnson, R.S. HIF transcription factors, inflammation, and immunity. *Immunity* **41**, 518-528 (2014).
52. Maxwell, P.J. *et al.* HIF-1 and NF-kappaB-mediated upregulation of CXCR1 and CXCR2 expression promotes cell survival in hypoxic prostate cancer cells. *Oncogene* **26**, 7333-7345 (2007).
53. Liu, X., He, L., Stensaas, L., Dinger, B. & Fidone, S. Adaptation to chronic hypoxia involves immune cell invasion and increased expression of inflammatory cytokines in rat carotid body. *Am J Physiol Lung Cell Mol Physiol* **296**, L158-166 (2009).
54. Yoshida, D., Kim, K., Noha, M. & Teramoto, A. Hypoxia inducible factor 1-alpha regulates of platelet derived growth factor-B in human glioblastoma cells. *J Neurooncol* **76**, 13-21 (2006).
55. Kaelin, W.G., Jr. ROS: really involved in oxygen sensing. *Cell Metab* **1**, 357-358 (2005).
56. Kim, K.S., Rajagopal, V., Gonsalves, C., Johnson, C. & Kalra, V.K. A novel role of hypoxia-inducible factor in cobalt chloride- and hypoxia-mediated expression of IL-8 chemokine in human endothelial cells. *J Immunol* **177**, 7211-7224 (2006).
57. Welford, S.M. & Giaccia, A.J. Hypoxia and senescence: the impact of oxygenation on tumor suppression. *Mol Cancer Res* **9**, 538-544 (2011).
58. Chandel, N.S. *et al.* Reactive oxygen species generated at mitochondrial complex III stabilize hypoxia-inducible factor-1alpha during hypoxia: a mechanism of O2 sensing. *J Biol Chem* **275**, 25130-25138 (2000).
59. Cheng, G., Diebold, B.A., Hughes, Y. & Lambeth, J.D. Nox1-dependent reactive oxygen generation is regulated by Rac1. *J Biol Chem* **281**, 17718-17726 (2006).
60. van Haren, J. *et al.* Dynamic microtubules catalyze formation of navigator-TRIO complexes to regulate neurite extension. *Curr Biol* **24**, 1778-1785 (2014).
61. Mizrahi, A. *et al.* Activation of the phagocyte NADPH oxidase by Rac Guanine nucleotide exchange factors in conjunction with ATP and nucleoside diphosphate kinase. *J Biol Chem* **280**, 3802-3811 (2005).
62. Ganem, N.J. *et al.* Cytokinesis failure triggers hippo tumor suppressor pathway activation. *Cell* **158**, 833-848 (2014).
63. Abo, A. *et al.* Activation of the NADPH oxidase involves the small GTP-binding protein p21rac1. *Nature* **353**, 668-670 (1991).
64. Halliwell, B. & Gutteridge, J.M.C. *Free radicals in biology and medicine*, Edn. Fifth edition. (Oxford University Press, Oxford, United Kingdom ;; 2015).
65. Kaewpila, S., Venkataraman, S., Buettner, G.R. & Oberley, L.W. Manganese superoxide dismutase modulates hypoxia-inducible factor-1 alpha induction via superoxide. *Cancer Res* **68**, 2781-2788 (2008).
66. Goyal, P. *et al.* Upregulation of NAD(P)H oxidase 1 in hypoxia activates hypoxia-inducible factor 1 via increase in reactive oxygen species. *Free Radic Biol Med* **36**, 1279-1288 (2004).

67. Moeller, B.J., Cao, Y., Li, C.Y. & Dewhirst, M.W. Radiation activates HIF-1 to regulate vascular radiosensitivity in tumors: role of reoxygenation, free radicals, and stress granules. *Cancer Cell* **5**, 429-441 (2004).
68. Chan, D.A., Sutphin, P.D., Denko, N.C. & Giaccia, A.J. Role of prolyl hydroxylation in oncogenically stabilized hypoxia-inducible factor-1alpha. *J Biol Chem* **277**, 40112-40117 (2002).
69. Acosta, J.C. *et al.* A complex secretory program orchestrated by the inflammasome controls paracrine senescence. *Nat Cell Biol* **15**, 978-990 (2013).
70. Vitre, B. *et al.* Chronic centrosome amplification without tumorigenesis. *Proc Natl Acad Sci U S A* **112**, E6321-6330 (2015).
71. Kulukian, A. *et al.* Epidermal development, growth control, and homeostasis in the face of centrosome amplification. *Proc Natl Acad Sci U S A* **112**, E6311-6320 (2015).
72. Cho, H. *et al.* On-target efficacy of a HIF-2alpha antagonist in preclinical kidney cancer models. *Nature* **539**, 107-111 (2016).
73. Dobin, A. *et al.* STAR: ultrafast universal RNA-seq aligner. *Bioinformatics* **29**, 15-21 (2013).
74. DeLuca, D.S. *et al.* RNA-SeQC: RNA-seq metrics for quality control and process optimization. *Bioinformatics* **28**, 1530-1532 (2012).
75. Liao, Y., Smyth, G.K. & Shi, W. featureCounts: an efficient general purpose program for assigning sequence reads to genomic features. *Bioinformatics* **30**, 923-930 (2014).
76. Anders, S. & Huber, W. Differential expression analysis for sequence count data. *Genome Biol* **11**, R106 (2010).
77. Papathanasiou, S. *et al.* Tumor necrosis factor-alpha confers cardioprotection through ectopic expression of keratins K8 and K18. *Nat Med* **21**, 1076-1084 (2015).
78. Liberzon, A. *et al.* The Molecular Signatures Database (MSigDB) hallmark gene set collection. *Cell Syst* **1**, 417-425 (2015).
79. Liberzon, A. *et al.* Molecular signatures database (MSigDB) 3.0. *Bioinformatics* **27**, 1739-1740 (2011).

METHODS

Cell culture All source cell culture was maintained in media containing plasmocin (1:5000 dilution, Invivogen) to prevent mycoplasma contamination. Culture plates were briefly coated with 40µg/ml of fibronectin (Sigma) and glass coverslips were incubated in 40 µg/ml fibronectin for at least 2 hours. Human mammary epithelial MCF10A cells were maintained at 37^0C with 5% CO_2 atmosphere and cultured as previously described[7]. In brief, MCF10A cells were cultured in phenol red-free DMEM/F12 (Invitrogen) supplemented with 5% horse serum (Sigma), 20ng/ml epidermal growth factor (EGF; Sigma), 10mg/ml insulin (Invitrogen), 100 mg/ml hydrocortisone (Sigma), 1ng/ml cholera toxin (Sigma) and 100 IU/ml penicillin and 100 µg/ml streptomycin (Invitrogen). Telomerase-immortalized RPE-1 cells (ATCC), and all derivative cell lines generated in this study were cultured in phenol red-free DMEM/F12 media containing 10% FBS, 100U/ml penicillin, and 100µg/ml streptomycin. RPE-1 cells were maintained at 37°C in 5% CO_2 atmosphere. For experiments performed in physiological normoxia, RPE-1 cells were maintained at 5% O_2 conditions in a custom-designed hypoxia chamber (Coy Labs).

To conditionally overexpress PLK4, lentiviral vectors pLenti-CMV-TetR-Blast (17492, Addgene) and pLenti-CMV/TO-Neo-Dest (17292, Addgene) were used. Wild-type PLK4 and PLK4 1–608 cDNAs (control 608) were cloned using the Gateway system into the pLenti-CMV/TO-Neo-Dest vector Cells were coinfected with a lentivirus containing the TetR and with the lentivirus containing the wild-type PLK4 or control 608 open reading frames. Transduced cells were selected with Blasticidin (10 µg/ml) and Geneticin (200µg/ml). control 608 and PLK4 overexpression was induced transiently. Transduced cells that survive the selection are used for subsequent experiments and a maintenance dose of 5 µg/ml of Blasticidin and 80µg/ml of Geneticin was used in stock cultures.

Generation of tetraploids and 'evolved' tetraploids with normal centrosome numbers To generate G1 arrested tetraploids, 15cm dishes were seeded with 6 million exponentially growing RPE1-FUCCI cells, such that they were ~65% confluent the following day. Day 2: 4 µM Dihydrocytochalasin B (DCB) was added to each 15 cm dish for 16 hr. Day 3: DCB-treated cells were washed 5 times for 5 minutes, incubated in medium containing 2.5 µg/ml Hoechst dye for 1 hr, then trypsinized in 0.05% trypsin. G1 diploids (2C DNA content; mCherry+, GFP−) and G1 tetraploids (4C DNA content; mCherry+, GFP−) were isolated by FACS sorting. FACS sorted cells were seeded on 6 well plates coated with 40µg/ml fibronectin.

Evolved tetraploid RPE-1 cells, kindly provided by Huadi Zhang, with the normal number of centrosomes were derived as described[33]. Briefly, tetraploid RPE-1 cells were treated for 16 hr with 0.2 μm cytochalasin D, and FACS-sorted by DNA content using Hoechst staining (Molecular Probes). The peak of cells with a DNA content of 8C were isolated and cultured for ∼1 week before a second iteration of the FACS sorting to re-isolate 8C cells. A total of 5 purifying sorts for ∼6 weeks was required to generate a pure population of proliferating tetraploid cells with normal centrosome numbers.

Induction of centrosome amplification and senescence At day 0, control 608 and PLK4 cells were gently dissociated into single cells, then seeded at low density into media with 2μg/ml of doxycycline such that they were ~80% confluent on day 5. After ~48 hours of doxycycline incubation, the culture media with doxycycline was replaced. At day 5, cells are gently dissociated into single cells before reseeding into 6 well plates to ~80% confluent on day 7. Because control 608 cells grow faster than PLK4 induced cells, control 608 cells are seeded at ~2.5 times lower density than PLK4 induced cells. Cells at ~80% confluency are analyzed either at day 7 or day 8. Media is left unchanged for ~3 days before analysis.

Mouse lines and RNA purification from tissues Control and PLK4 overexpressing mice were bred and maintained as previously described[6]. Quick-frozen skin samples were pulverized with a Cryoprep Impactor (Covaris). RNA purification was then performed with the RNeasy kit (Qiagen) according to manufacturer's instructions.

Antibodies, siRNA and drugs Primary antibodies used in this study were: mouse monoclonal antibodies against Centrin (1:500 for immunofluorescence; Merck Millipore catalogue number 04-1624, clone number 20H5), mouse monoclonal antibodies against ANGPTL4 (1:50 for western blotting; Santa Cruz catalogue number sc-373762, clone number C-7), rabbit polyclonal antibodies against Trio, was a gift from A.Debant (University of Montpellier, France, 1:500 for western blotting), mouse monoclonal antibodies against Rb (Thermo Fisher Scientific catalogue number: BDB554136, clone number G3-245), rabbit polyclonal antibodies against phosphoRb Ser780 (catalogue number 9307S), mouse monoclonal antibodies against GAPDH (1:10000 for western blotting; Abcam catalogue number ab8245), rabbit polyclonal antibodies against GAPDH (1:10000 for western blotting; Abcam catalogue number ab9485), mouse monoclonal antibodies HIF-1α (1:100 for western blotting; BD Transduction Laboratories catalogue number 610959, clone number 54) mouse monoclonal antibodies against HIF-1α (1:50-1:100 for immunofluorescence; Abcam catalogue number ab16066), rabbit polyclonal antibodies against

phosphoH2AX (1:500 for immunofluorescence; EMD Millipore Upstate catalogue number 05-636-I, Clone: JBW301), rabbit polyclonal antibodies against p65/RELA (1:500 for immunofluorescence; Santa Cruz Biotechnology catalogue number sc-372), mouse monoclonal antibodies against CYBA (1:100 for western blotting; Santa Cruz catalogue number sc-271968), Mouse IgG antibody (Abcam, ab37355) was used at 40μg/ml as control for blocking experiments. The ANGPTL4 mouse antibody mAb11F6C4, used at 40μg/ml for blocking experiments, was a gift from Tan Nguan Soon, Andrew (Lee Kong Chian School of Medicine, Nanyang Technological University, Singapore). siRNA against CYBA p22phox (Dharmacon, L-011020-02)

Doxycycline (Sigma Aldrich catalogue number D3072) was used at 2 mg/ml. Catalase (Sigma Aldrich (catalogue number: C9322) was used at 2U/μl for 24 hours. TNFα (Roche Diagnostics catalogue number: 11371843001) was used at 20ng/ml for 2 hours. The following doses of inhibitors were used: 50 μM NSC23766 (EMD Millipore), 4μM of dihydrocytochalasin B (DCB; Sigma), 40 ng/ml Doxorubicin (Sigma).

Immunofluorescence and microscopy Cells were fixed at 4°C with 4% paraformaldehyde in cytoskeleton stabilization buffer (10mM PIPES at pH 6.8, 100mM KCl, 300mM sucrose, 2mM EGTA and 2mM $MgCl_2$) on ice for 25 min and subsequently permeabilized with 0.2% Triton-X in PBS for 10 minutes at room temperature. Fixed cells were blocked with 5% BSA in TBS for overnight at 4°C. Primary antibodies were incubated for overnight at 4°C for HIF1α and 45 minutes room temperature for phosphoH2AX and p65/RELA. For centrin-1 staining, cells were fixed with -20°C methanol for 5 minutes on ice. For all immunostaining, secondary Alexa Fluor antibodies were incubated at room temperature for an hour.
Images were collected with Nikon Ti inverted microscope with 20x wide-field optics equipped with perfect focus system, a Hamamatsu ORCA ER cooled CCD camera controlled with Nikon NIS-Element software and an OkoLab 37°C, 5% CO_2 microscope chamber.

Matrigel-coated transwell invasion assay A previously described assay for Matrigel-coated transwell invasion assay was adapted for the current study as follows. 8μm Boyden chamber inserts were used (Cell Biolabs: CytoSelect Tumor Transwell ECM Migration Assay, Catalogue No. CBA-216). For the bottom chamber, MCF10A cells with or without centrosome amplification that were cultured for 48 hours in 400μl of full media was used. mCherry MDA-MB-468 cells were seeded on the top chamber. After overnight culture, cells on top of each insert were removed and the trans-well membrane was mounted

onto slides. Migration of mCherry MDA-MB-468 cells to the bottom of the membrane was visualized with a spinning disc microscope at 10x magnification.

Media Swap Motility Assay Cells were plated at 0.5-1x10^6 per well in 6 well plates and allowed to attach for 24h. Then, cells were starved in serum free medium for two hours and incubated in 0.5% horse serum media for another 12 hours. Conditioned medium from cells with or without centrosome amplification were collected and centrifuged at 5000 rpm for 20 minutes to eliminate any detached cells or debris. Conditioned medium was then added to cells and the effect of the swapped conditioned medium on the cellular motility was imaged with bright field microscopy (Nikon Ti).

CRISPR Knockouts and Lentiviral Transduction Puromycin selectable CRISPR lentiviruses were obtained commercially from Applied Biological Materials. Three different CRISPR lentiviruses were tested for each target genes. The CRISPR lentivirus that achieve the best knockout and the MCF10A knockout cells were characterized and used for subsequent experiments. The guide RNA targeting the sequences of the genes of interest and scrambled control is as follow. Scrambled control 5'-GCACTCACATCGCTACATCA-3' catalogue number K011, Trio Target Sequence 1: 5'-?? -3'; catalogue number K2470115, ANGPTL4 Target Sequence 3: 5'-AGGGGCTAACGGGAGGTCGG-3'; catalogue number K0085515

The previously described[72] HIF-1α pLenti-CRISPRv2 was a gift from William G. Kaelin, Jr. (Dana-Farber Cancer Institute, Boston, USA). The sgRNA sequence targeting HIF1α is as follow: 5'-CACCGTGTGAGTTCGCATCTTGATA -3'.
For lentivirus production, 6μg lentiviral constructs, 3 μg psPAX2 (Addgene), and 3 μg pMD2.G (Addgene) were transfected into 293T cells at 80% confluency in a 10-cm dish with 8 ml of media. 20 μl of lipofectamine 3000 (Life Technologies) was used and transfection was performed according to manufacturer's instructions. Virus was harvested at 48 hours and 72 hours post-infection, and filtered with a 0.2μm filter. MCF10A cells were infected for 12 hours, with virus containing the genes of interest in the presence of 10 μg/ml polybrene, washed thoroughly, and allowed to recover for 24 hours before any selection.

Image processing and analysis ImageJ macros are created to determine the nuclear to cytoplasmic ratio of fluorescence intensity and the number of phosphoH2AX foci in cells. For the quantification of nuclear and cytoplasmic mean fluorescence intensity of HIF-1α and p65, a nuclei mask was generated from the

Z-projection of the Hoescht nuclear staining and a 1 μm region surrounding the nucleus was designated as the cytoplasmic region. The watershed function was applied on the nuclei mask to ensure separation of overlapping nuclei.

For the quantification of γ-H2AX foci, a rolling-ball (5 pixels) background subtraction was applied to 8 bit images labelled for γ-H2AX. A nuclear mask generated from the Z-projection of the hoescht nuclear staining after watershed segmentation was used to identify the γ-H2AX foci within an individual nucleus. The 'Find Maxima' function on ImageJ was used to count the number of γ-H2AX foci in each nucleus. The noise for the γ-H2AX staining was obtained from cytoplasmic staining and set as the noise tolerance input on the 'Find Maxima' function.

Suspended Cell Size Measurement, SA-β-gal assays and Superoxide Assay Suspended Cell Size was determined using the coulter counter (Beckman, Vi-cell). SA-β-gal activity was determined using the Senescent Cell Staining Kit (Sigma), by staining SA-β-gal for overnight, according to manufacturer instructions. Cells positive for SA-β-gal were identified by visual scoring. Superoxide levels were measured using a superoxide assay (Abcam catalogue number: ab139476) according to manufacturer instructions.

NextSeq500 RNA Library Preparation and Sequencing RNA quantity was determined on the Qubit using the Qubit RNA Assay Kit (Life Tech) and RNA quality was determined on the Bioanalyzer using the RNA Pico Kit (Agilent). Using the NEB Next Ultra RNA Library Prep Kit for Illumina (NEB), which selects for poly(A) mRNA, 100ng of total RNA was used for cDNA library construction, according to the manufacturer's protocol. Following library construction, DNA quantity was determined using the Qubit High Sensitivity DNA Kit (Life Technologies) and library insert size was determined using the Bioanalyzer High Sensitivity Chip Kit (Agilent). Finally, qPCR was performed using the Universal Library Quantification Kit for Illumina (Kapa Biosystems) and ran on the 7900HT Fast qPCR machine (ABI) for quantification and normalization of libraries. Libraries that passed quality control were diluted to 2nM DNA content using sterile water and then sequenced on the NextSeq500 (Illumina) at a final concentration of 12pM, according to manufacturer's instructions.

RNA Sequencing Analysis Sequencing reads were aligned to the reference genome using the RNA-specific STAR aligner using default parameters[73]. The quality of the sequencing run and alignment was assessed by RNA-SeQC[74]. The featureCounts tool is used to count sequencing reads mapping to the

reference genome at the gene level[75]. The counts are subsequently normalized between samples using DESeq2 to control for experimental variation[76]. Differential expression analysis was performed between the desired experimental contrasts using DESeq2.

Ingenuity Pathway Analysis Meta-analysis of the DESeq2 analysed RNA sequencing data was performed to identify the top pathways that are statistically associated with the list of the significantly induced genes[77] (fold change $\geq$ 2, FDR q value < 0.05, using the Ingenuity Pathway Analysis platform IPA, Ingenuity Systems, Qiagen).

Gene Set Enrichment Analysis We used GSEA v3.0 to examine the association between gene sets and gene expression. Normalized read counts from DESeq2 analysis were used for GSEA. Genes with a 0 read count in either control or experimental group were excluded. GSEA was performed using gene sets as permutation type, 1,000 permutations and log2 ratio of classes as metric for ranking genes. We employ the hallmark gene sets from the Molecular Signatures Database (MSigDB)[32, 78, 79]. Hallmark gene sets summarize and represent specific well-defined biological states or processes and display coherent expression. These gene sets were generated by a computational methodology based on identifying gene set overlaps and retaining genes that display coordinate expression, thus reducing data noise and redundancy.
To construct a HIFα signature up gene set we performed RNA sequencing of MCF10A cells after overnight treatment with 1μm of DMOG, with DMSO treated cells as control. We included genes that were upregulated by DMOG in DESeq analysis (p(adjusted)<0.05, fold change $\geq$ 4, Supplementary Table 1).

Quantitative RT-PCR Total RNA was isolated using the RNAeasy Mini Kit (Qiagen), and cDNA was synthesized using SuperScript III (Invitrogen) according to manufacturer instructions. Quantitative RT-qPCR was performed in triplicate using SYBR Green (Life Technologies) on a ViiA 7 Real-Time PCR machine (Thermo Fisher Scientific) with GAPDH as an internal normalization control.

qPCR primers (PrimeTime® Predesigned qPCR Assays) purchased from IDT were used and product information were as follow: GAPDH, Assay ID: Hs.PT.39a.22214836; Angptl4, Assay ID: Mm.PT.58.12348309.

ELISA Cells were starved for 2 hours before reintroducing full media to collect cellular secretion. After 24 hours of incubation, the conditioned (full) media is collected and a protease inhibitor cocktail (Sigma)

was added to prevent protein degradation. The conditioned media was centrifuged for 10 minutes at 5000rpm to remove any cellular debris and subsequently quantified for ANGPTL4's concentration with ELISA (ELH-ANGPTL4, RayBiotech). The total cell number was used to normalize ANGPTL4's concentration across replicates.

Figure 1.

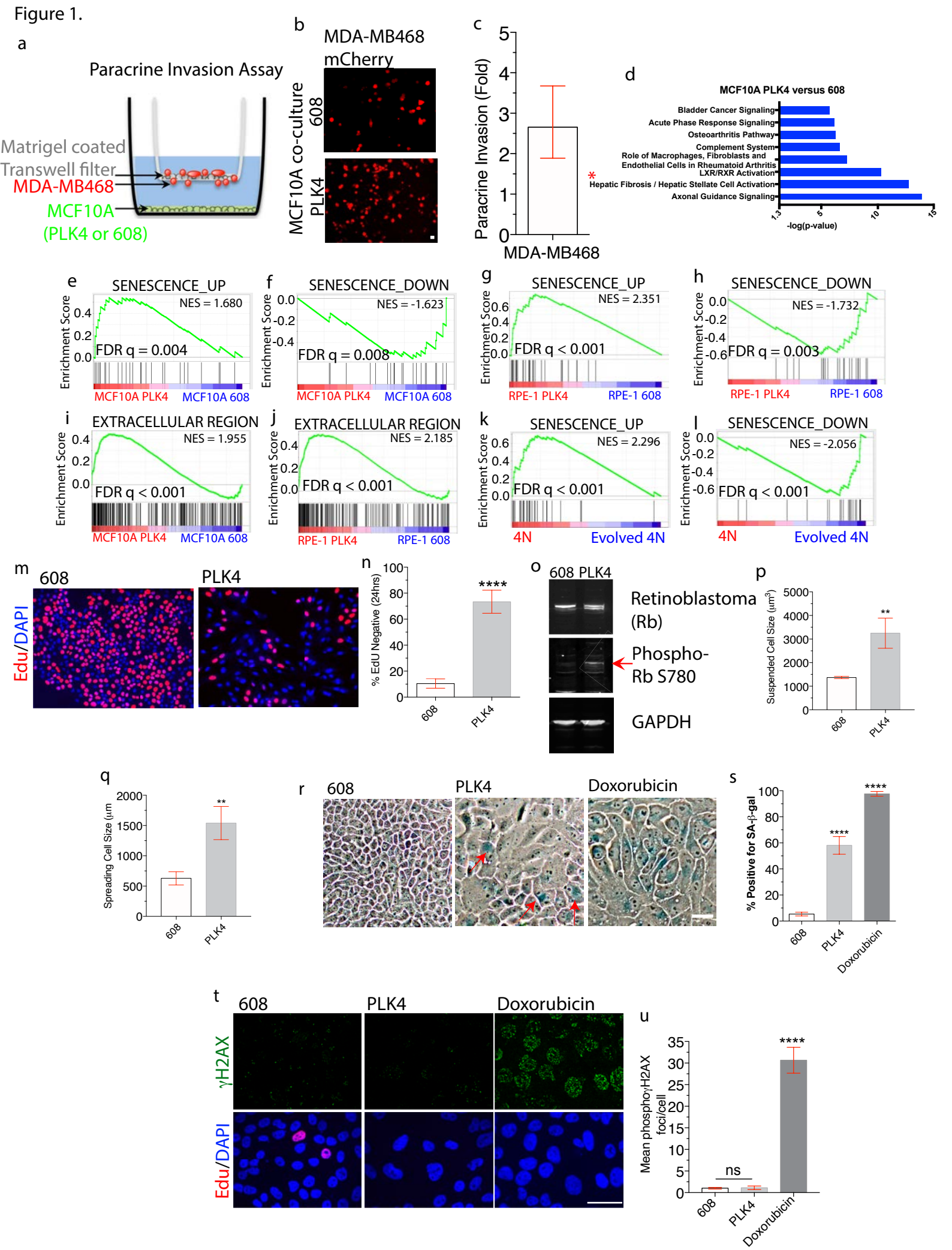
a
Paracrine Invasion Assay
Matrigel coated
Transwell filter
MDA-MB468
MCF10A
(PLK4 or 608)
b
MDA-MB468
mCherry
MCF10A co-culture
608
PLK4
c
Paracrine Invasion (Fold)
MDA-MB468
d
MCF10A PLK4 versus 608
Bladder Cancer Signaling
Acute Phase Response Signaling
Osteoarthritis Pathway
Complement System
Role of Macrophages, Fibroblasts and Endothelial Cells in Rheumatoid Arthritis
LXR/RXR Activation
Hepatic Fibrosis / Hepatic Stellate Cell Activation
Axonal Guidance Signaling
-log(p-value)
e
SENESCENCE_UP
NES = 1.680
FDR q = 0.004
MCF10A PLK4
MCF10A 608
f
SENESCENCE_DOWN
NES = -1.623
FDR q = 0.008
MCF10A PLK4
MCF10A 608
g
SENESCENCE_UP
NES = 2.351
FDR q < 0.001
RPE-1 PLK4
RPE-1 608
h
SENESCENCE_DOWN
NES = -1.732
FDR q = 0.003
RPE-1 PLK4
RPE-1 608
i
EXTRACELLULAR REGION
NES = 1.955
FDR q < 0.001
MCF10A PLK4
MCF10A 608
j
EXTRACELLULAR REGION
NES = 2.185
FDR q < 0.001
RPE-1 PLK4
RPE-1 608
k
SENESCENCE_UP
NES = 2.296
FDR q < 0.001
4N
Evolved 4N
l
SENESCENCE_DOWN
NES = -2.056
FDR q < 0.001
4N
Evolved 4N
Enrichment Score
m
608
PLK4
Edu/DAPI
n
% EdU Negative (24hrs)
608
PLK4
o
608 PLK4
Retinoblastoma (Rb)
Phospho-Rb S780
GAPDH
p
Suspended Cell Size (µm³)
608
PLK4
q
Spreading Cell Size (µm)
608
PLK4
r
608
PLK4
Doxorubicin
s
% Positive for SA-β-gal
608
PLK4
Doxorubicin
t
608
PLK4
Doxorubicin
γH2AX
Edu/DAPI
u
Mean phosphoγH2AX foci/cell
ns
608
PLK4
Doxorubicin

Figure 2

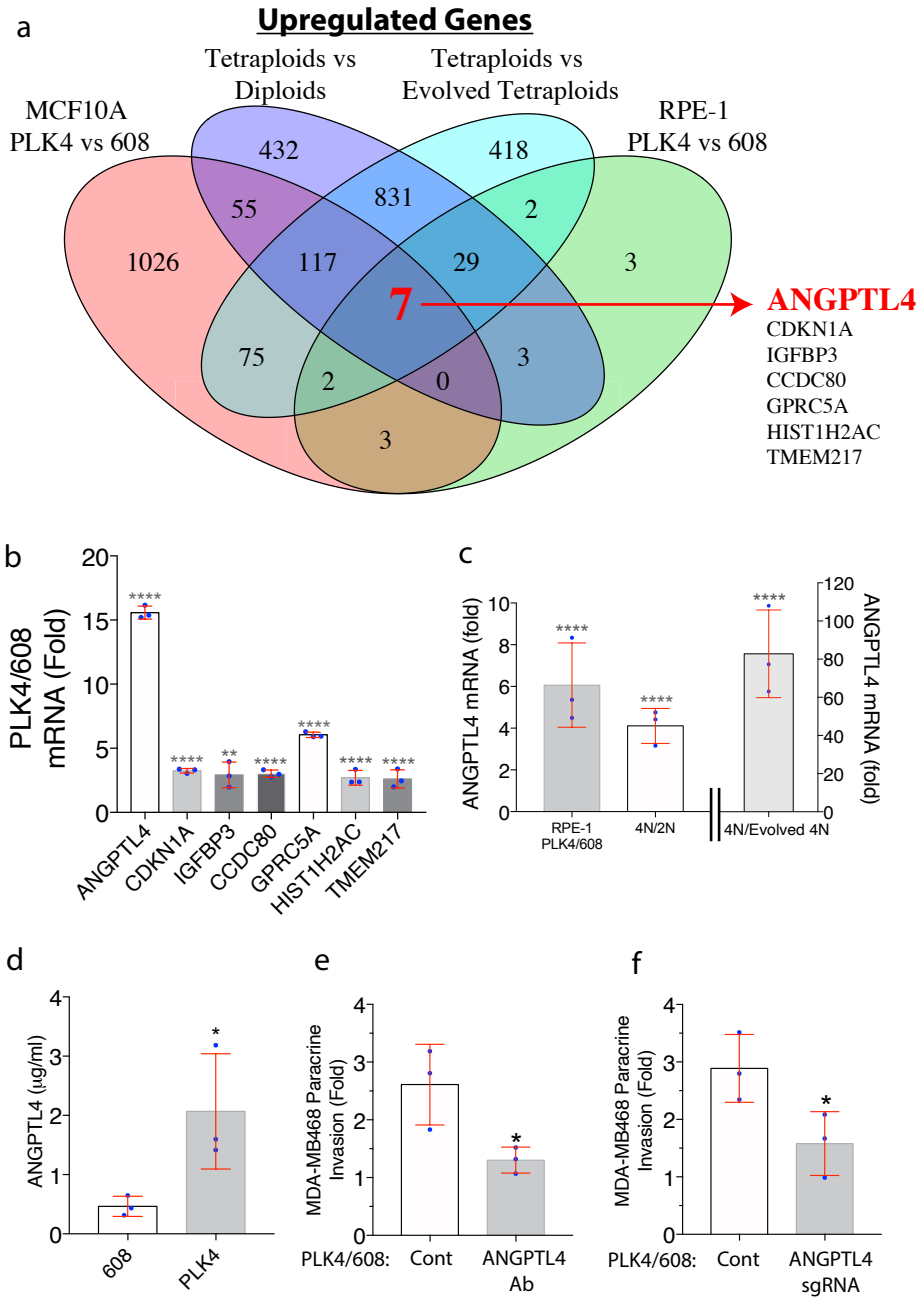
a
Upregulated Genes
MCF10A
PLK4 vs 608
Tetraploids vs
Diploids
Tetraploids vs
Evolved Tetraploids
RPE-1
PLK4 vs 608
1026
432
418
3
55
831
2
117
29
7
75
3
2
0
3
ANGPTL4
CDKN1A
IGFBP3
CCDC80
GPRC5A
HIST1H2AC
TMEM217
b
PLK4/608
mRNA (Fold)
ANGPTL4
CDKN1A
IGFBP3
CCDC80
GPRC5A
HIST1H2AC
TMEM217
c
ANGPTL4 mRNA (fold)
RPE-1
PLK4/608
4N/2N
4N/Evolved 4N
d
ANGPTL4 (µg/ml)
608
PLK4
e
MDA-MB468 Paracrine
Invasion (Fold)
PLK4/608:
Cont
ANGPTL4
Ab
f
MDA-MB468 Paracrine
Invasion (Fold)
PLK4/608:
Cont
ANGPTL4
sgRNA

Figure 3

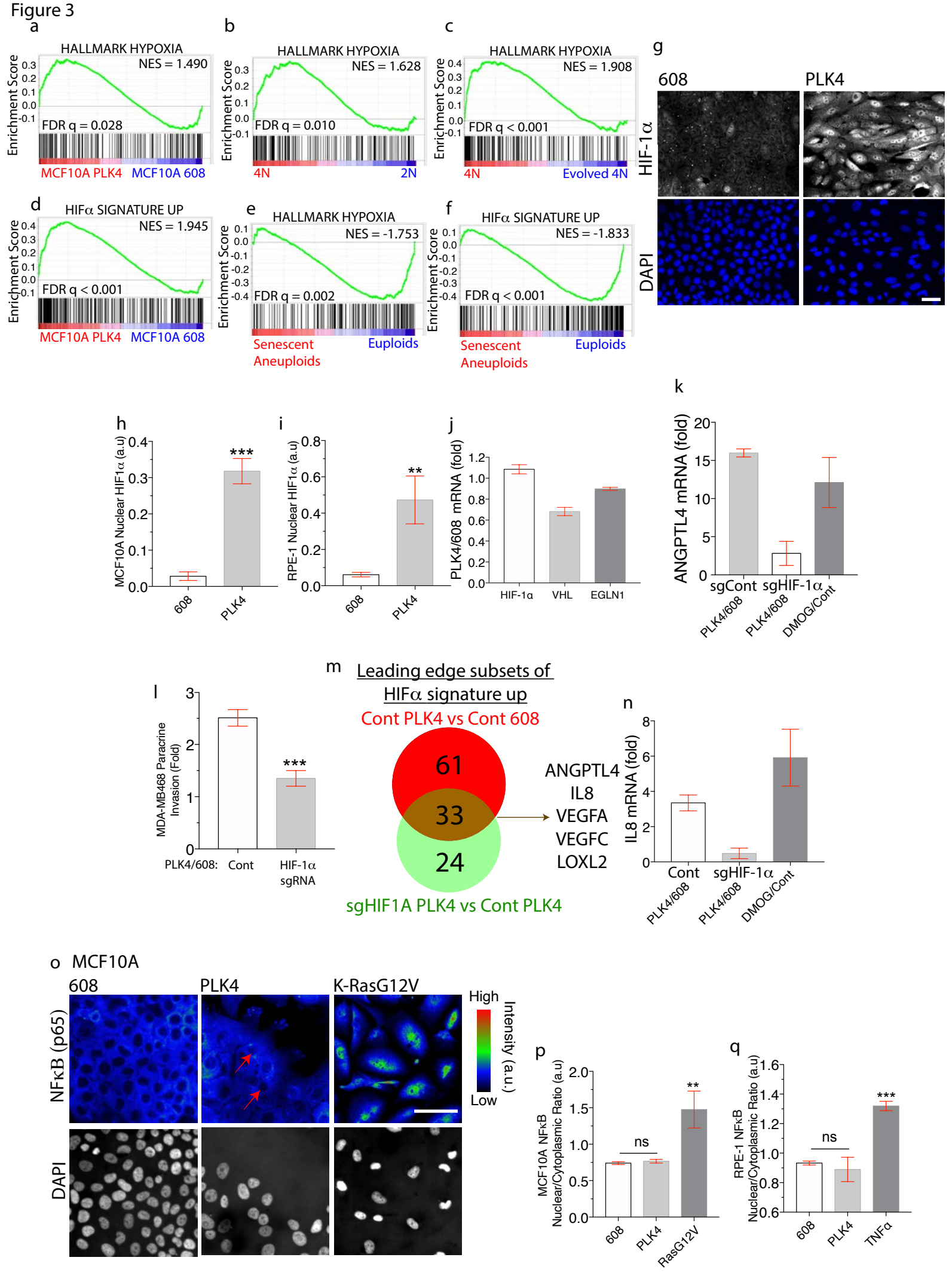
a
HALLMARK HYPOXIA
NES = 1.490
FDR q = 0.028
Enrichment Score
MCF10A PLK4
MCF10A 608
b
HALLMARK HYPOXIA
NES = 1.628
FDR q = 0.010
4N
2N
c
HALLMARK HYPOXIA
NES = 1.908
FDR q < 0.001
4N
Evolved 4N
d
HIFα SIGNATURE UP
NES = 1.945
FDR q < 0.001
MCF10A PLK4
MCF10A 608
e
HALLMARK HYPOXIA
NES = -1.753
FDR q = 0.002
Senescent Aneuploids
Euploids
f
HIFα SIGNATURE UP
NES = -1.833
FDR q < 0.001
Senescent Aneuploids
Euploids
g
608
PLK4
HIF-1α
DAPI
h
MCF10A Nuclear HIF1α (a.u)
608
PLK4
i
RPE-1 Nuclear HIF1α (a.u)
608
PLK4
j
PLK4/608 mRNA (fold)
HIF-1α
VHL
EGLN1
k
ANGPTL4 mRNA (fold)
sgCont
sgHIF-1α
PLK4/608
PLK4/608
DMOG/Cont
l
MDA-MB468 Paracrine Invasion (Fold)
PLK4/608:
Cont
HIF-1α sgRNA
m
Leading edge subsets of HIFα signature up
Cont PLK4 vs Cont 608
61
33
24
sgHIF1A PLK4 vs Cont PLK4
ANGPTL4
IL8
VEGFA
VEGFC
LOXL2
n
IL8 mRNA (fold)
Cont
sgHIF-1α
PLK4/608
PLK4/608
DMOG/Cont
o MCF10A
608
PLK4
K-RasG12V
NFκB (p65)
DAPI
High
Low
Intensity (a.u.)
p
MCF10A NFκB Nuclear/Cytoplasmic Ratio (a.u)
ns
608
PLK4
RasG12V
q
RPE-1 NFκB Nuclear/Cytoplasmic Ratio (a.u)
ns
608
PLK4
TNFα

Figure 4

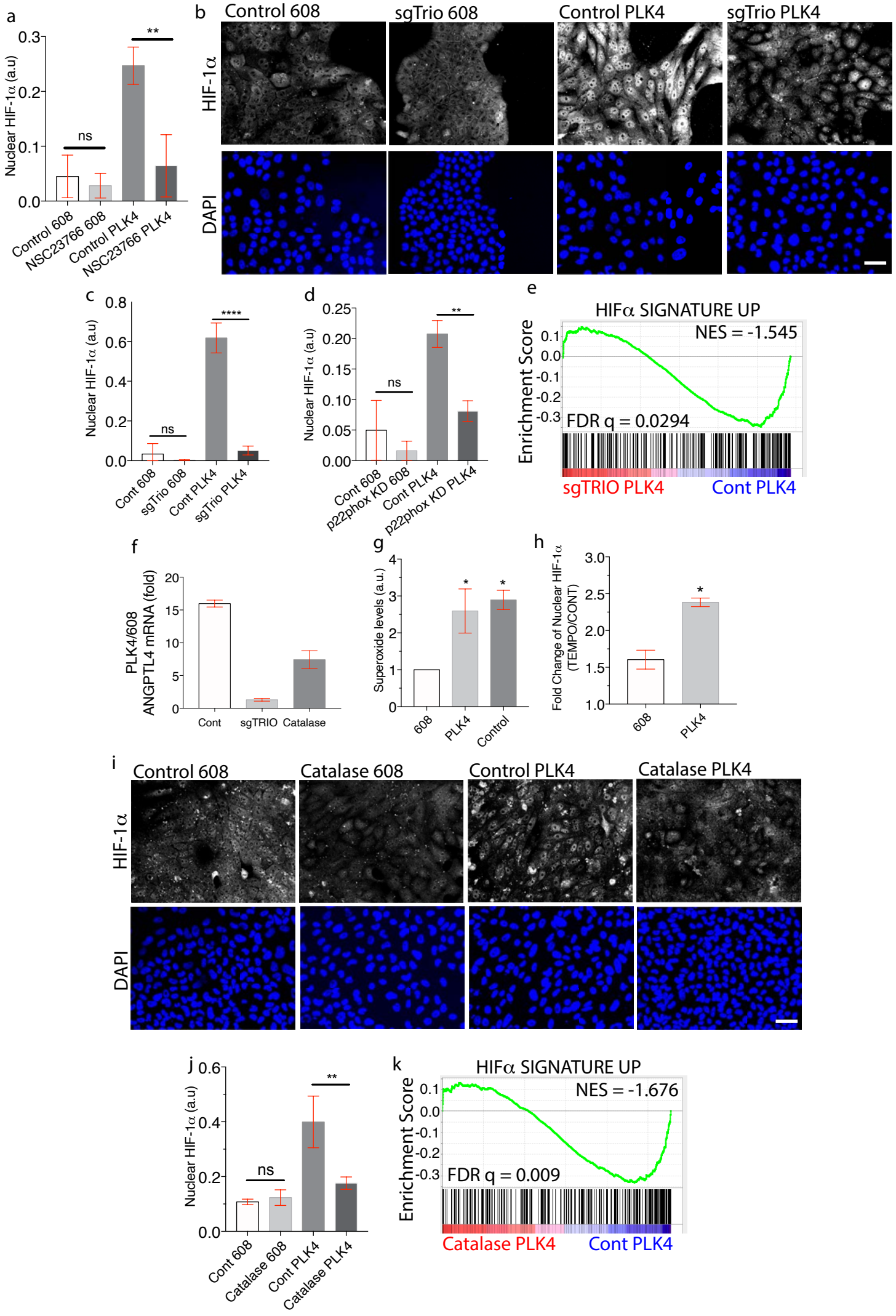
a
Nuclear HIF-1α (a.u)
0.3
0.2
0.1
0.0
ns
**
Control 608
NSC23766 608
Control PLK4
NSC23766 PLK4
b
Control 608
sgTrio 608
Control PLK4
sgTrio PLK4
HIF-1α
DAPI
c
Nuclear HIF-1α (a.u)
0.8
0.6
0.4
0.2
0.0
ns
****
Cont 608
sgTrio 608
Cont PLK4
sgTrio PLK4
d
Nuclear HIF-1α (a.u)
0.25
0.20
0.15
0.10
0.05
0.00
ns
**
Cont 608
p22phox KD 608
Cont PLK4
p22phox KD PLK4
e
HIFα SIGNATURE UP
NES = -1.545
Enrichment Score
0.1
0.0
-0.1
-0.2
-0.3
FDR q = 0.0294
sgTRIO PLK4
Cont PLK4
f
PLK4/608
ANGPTL4 mRNA (fold)
20
15
10
5
0
Cont
sgTRIO
Catalase
g
Superoxide levels (a.u.)
4
3
2
1
0
*
*
608
PLK4
Control
h
Fold Change of Nuclear HIF-1α
(TEMPO/CONT)
3.0
2.5
2.0
1.5
1.0
*
608
PLK4
i
Control 608
Catalase 608
Control PLK4
Catalase PLK4
HIF-1α
DAPI
j
Nuclear HIF-1α (a.u)
0.6
0.4
0.2
0.0
ns
**
Cont 608
Catalase 608
Cont PLK4
Catalase PLK4
k
HIFα SIGNATURE UP
NES = -1.676
Enrichment Score
0.1
0.0
-0.1
-0.2
-0.3
FDR q = 0.009
Catalase PLK4
Cont PLK4

Figure S1.

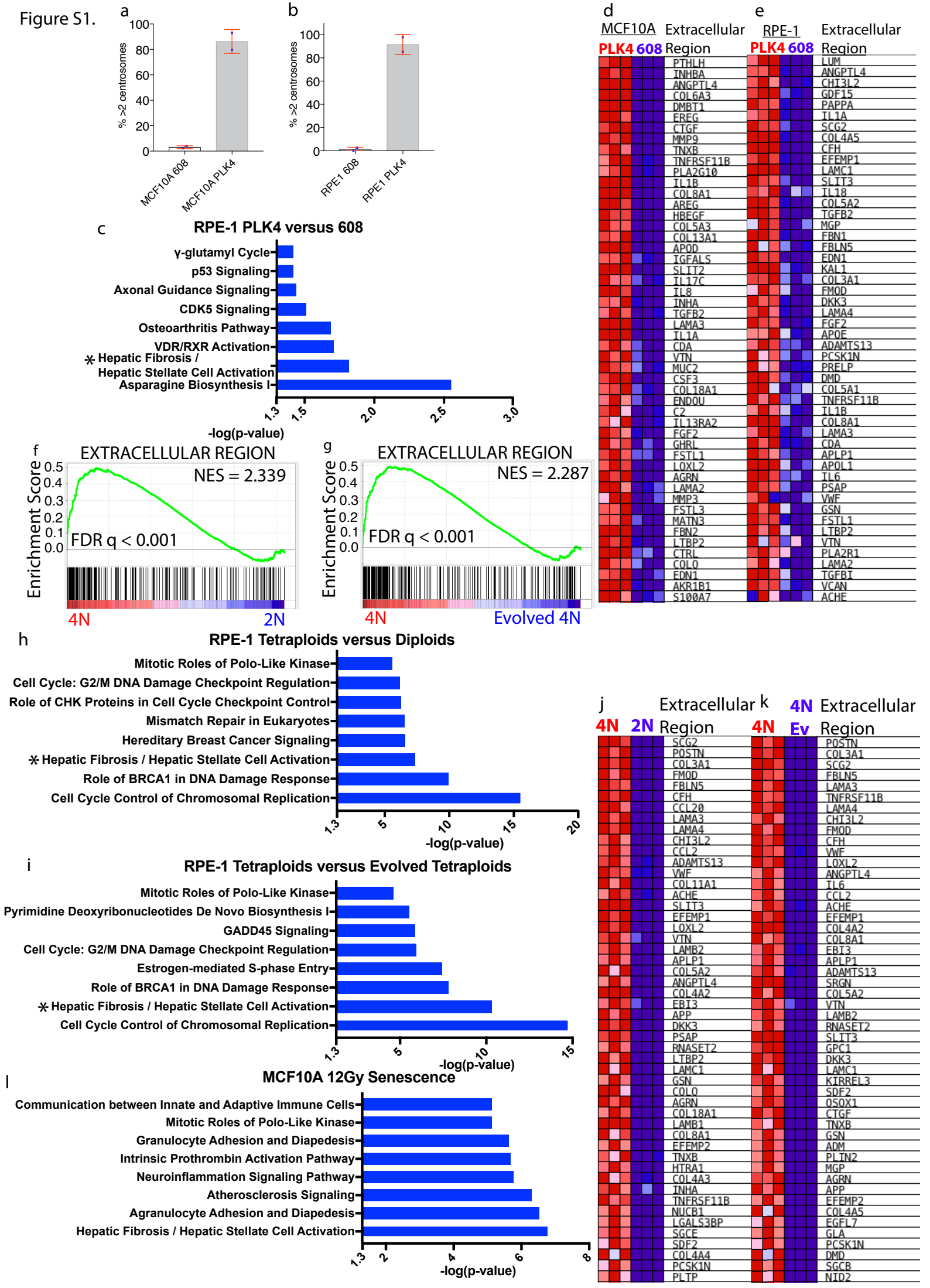
a
% >2 centrosomes
100
80
60
40
20
0
MCF10A 608
MCF10A PLK4
b
% >2 centrosomes
RPE1 608
RPE1 PLK4
c
RPE-1 PLK4 versus 608
γ-glutamyl Cycle
p53 Signaling
Axonal Guidance Signaling
CDK5 Signaling
Osteoarthritis Pathway
VDR/RXR Activation
Hepatic Fibrosis / Hepatic Stellate Cell Activation
Asparagine Biosynthesis I
1.3
1.5
2.0
2.5
3.0
-log(p-value)
d
MCF10A
PLK4 608
Extracellular Region
PTHLH
INHBA
ANGPTL4
COL6A3
DMBT1
EREG
CTGF
MMP9
TNXB
TNFRSF11B
PLA2G10
IL1B
COL8A1
AREG
HBEGF
COL5A3
COL13A1
APOD
IGFALS
SLIT2
IL17C
IL8
INHA
TGFB2
LAMA3
IL1A
CDA
VTN
MUC2
CSF3
COL18A1
ENDOU
C2
IL13RA2
FGF2
GHRL
FSTL1
LOXL2
AGRN
LAMA2
MMP3
FSTL3
MATN3
FBN2
LTBP2
CTRL
COLQ
EDN1
AKR1B1
S100A7
e
RPE-1
PLK4 608
Extracellular Region
LUM
ANGPTL4
CHI3L2
GDF15
PAPPA
IL1A
SCG2
COL4A5
CFH
EFEMP1
LAMC1
SLIT3
IL18
COL5A2
TGFB2
MGP
FBN1
FBLN5
EDN1
KAL1
COL3A1
FMOD
DKK3
LAMA4
FGF2
APOE
ADAMTS13
PCSK1N
PRELP
DMD
COL5A1
TNFRSF11B
IL1B
COL8A1
LAMA3
CDA
APLP1
APOL1
IL6
PSAP
VWF
GSN
FSTL1
LTBP2
VTN
PLA2R1
LAMA2
TGFBI
VCAN
ACHE
f
EXTRACELLULAR REGION
Enrichment Score
NES = 2.339
FDR q < 0.001
4N
2N
g
EXTRACELLULAR REGION
Enrichment Score
NES = 2.287
FDR q < 0.001
4N
Evolved 4N
h
RPE-1 Tetraploids versus Diploids
Mitotic Roles of Polo-Like Kinase
Cell Cycle: G2/M DNA Damage Checkpoint Regulation
Role of CHK Proteins in Cell Cycle Checkpoint Control
Mismatch Repair in Eukaryotes
Hereditary Breast Cancer Signaling
Hepatic Fibrosis / Hepatic Stellate Cell Activation
Role of BRCA1 in DNA Damage Response
Cell Cycle Control of Chromosomal Replication
1.3
5
10
15
20
-log(p-value)
i
RPE-1 Tetraploids versus Evolved Tetraploids
Mitotic Roles of Polo-Like Kinase
Pyrimidine Deoxyribonucleotides De Novo Biosynthesis I
GADD45 Signaling
Cell Cycle: G2/M DNA Damage Checkpoint Regulation
Estrogen-mediated S-phase Entry
Role of BRCA1 in DNA Damage Response
Hepatic Fibrosis / Hepatic Stellate Cell Activation
Cell Cycle Control of Chromosomal Replication
1.3
5
10
15
-log(p-value)
l
MCF10A 12Gy Senescence
Communication between Innate and Adaptive Immune Cells
Mitotic Roles of Polo-Like Kinase
Granulocyte Adhesion and Diapedesis
Intrinsic Prothrombin Activation Pathway
Neuroinflammation Signaling Pathway
Atherosclerosis Signaling
Agranulocyte Adhesion and Diapedesis
Hepatic Fibrosis / Hepatic Stellate Cell Activation
1.3
2
4
6
8
-log(p-value)
j
4N 2N
Extracellular Region
SCG2
POSTN
COL3A1
FMOD
FBLN5
CFH
CCL20
LAMA3
LAMA4
CHI3L2
CCL2
ADAMTS13
VWF
COL11A1
ACHE
SLIT3
EFEMP1
LOXL2
VTN
LAMB2
APLP1
COL5A2
ANGPTL4
COL4A2
EBI3
APP
DKK3
PSAP
RNASET2
LTBP2
LAMC1
GSN
COLQ
AGRN
COL18A1
LAMB1
COL8A1
EFEMP2
TNXB
HTRA1
COL4A3
INHA
TNFRSF11B
NUCB1
LGALS3BP
SGCE
SDF2
COL4A4
PCSK1N
PLTP
k
4N Ev
Extracellular Region
POSTN
COL3A1
SCG2
FBLN5
LAMA3
TNFRSF11B
LAMA4
CHI3L2
FMOD
CFH
VWF
LOXL2
ANGPTL4
IL6
CCL2
ACHE
EFEMP1
COL4A2
COL8A1
EBI3
APLP1
ADAMTS13
SRGN
COL5A2
VTN
LAMB2
RNASET2
SLIT3
GPC1
DKK3
LAMC1
KIRREL3
SDF2
QSOX1
CTGF
TNXB
GSN
ADM
PLIN2
MGP
AGRN
APP
EFEMP2
COL4A5
EGFL7
GLA
PCSK1N
DMD
SGCB
NID2

Figure S2

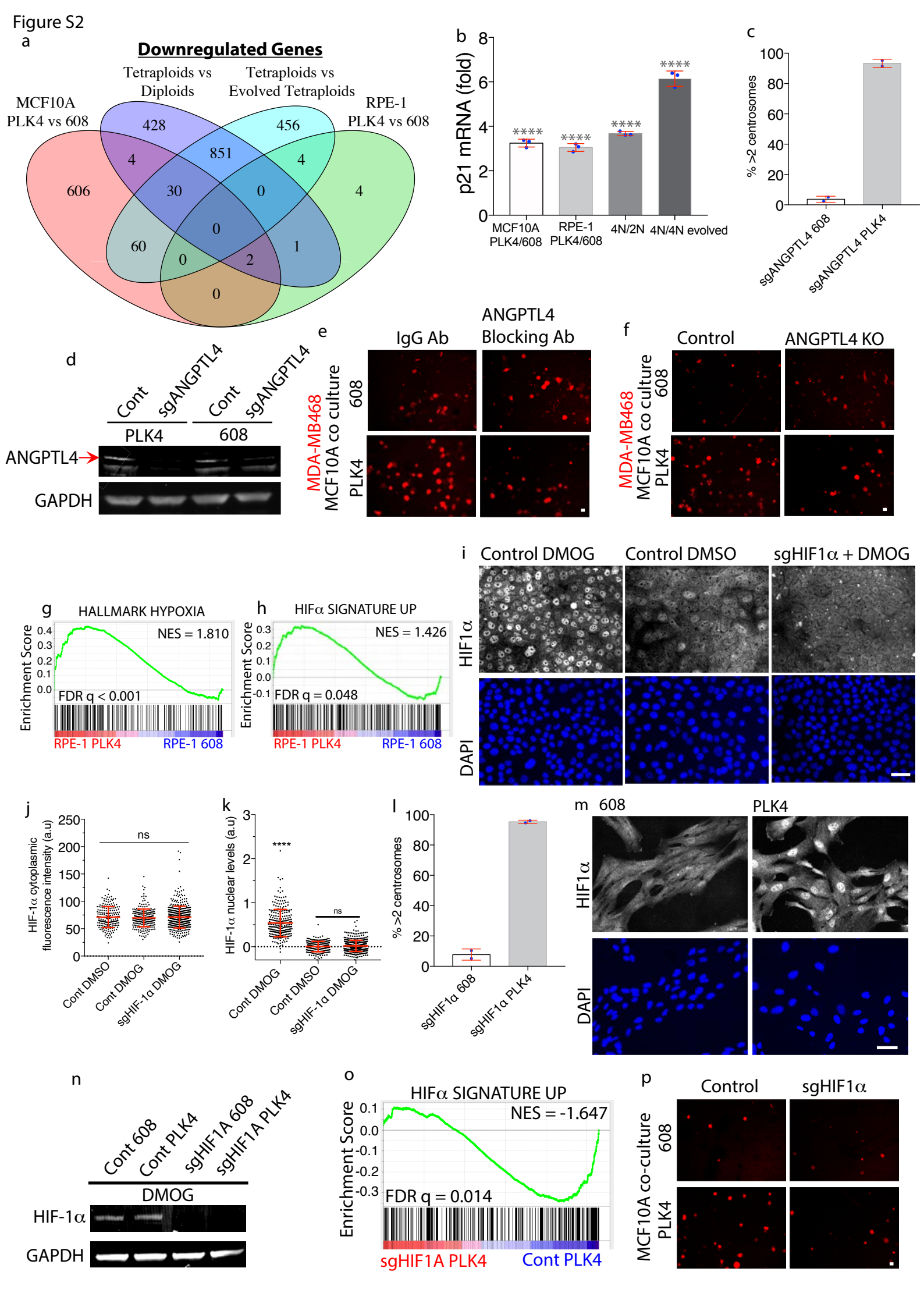
a
Downregulated Genes
Tetraploids vs Diploids
Tetraploids vs Evolved Tetraploids
MCF10A PLK4 vs 608
RPE-1 PLK4 vs 608
428
456
4
851
4
606
30
0
4
0
60
1
0
2
0
b
p21 mRNA (fold)
MCF10A PLK4/608
RPE-1 PLK4/608
4N/2N
4N/4N evolved
****
c
% >2 centrosomes
sgANGPTL4 608
sgANGPTL4 PLK4
d
Cont
sgANGPTL4
PLK4
608
ANGPTL4
GAPDH
e
IgG Ab
ANGPTL4 Blocking Ab
MDA-MB468
MCF10A co culture
608
PLK4
f
Control
ANGPTL4 KO
MDA-MB468
MCF10A co culture
608
PLK4
g
HALLMARK HYPOXIA
NES = 1.810
FDR q < 0.001
Enrichment Score
RPE-1 PLK4
RPE-1 608
h
HIFα SIGNATURE UP
NES = 1.426
FDR q = 0.048
Enrichment Score
RPE-1 PLK4
RPE-1 608
i
Control DMOG
Control DMSO
sgHIF1α + DMOG
HIF1α
DAPI
j
HIF-1α cytoplasmic fluorescence intensity (a.u)
ns
Cont DMSO
Cont DMOG
sgHIF-1α DMOG
k
HIF-1α nuclear levels (a.u)
****
ns
Cont DMOG
Cont DMSO
sgHIF-1α DMOG
l
% >2 centrosomes
sgHIF1α 608
sgHIF1α PLK4
m
608
PLK4
HIF1α
DAPI
n
Cont 608
Cont PLK4
sgHIF1A 608
sgHIF1A PLK4
DMOG
HIF-1α
GAPDH
o
HIFα SIGNATURE UP
NES = -1.647
FDR q = 0.014
Enrichment Score
sgHIF1A PLK4
Cont PLK4
p
Control
sgHIF1α
MCF10A co-culture
608
PLK4

Figure S3

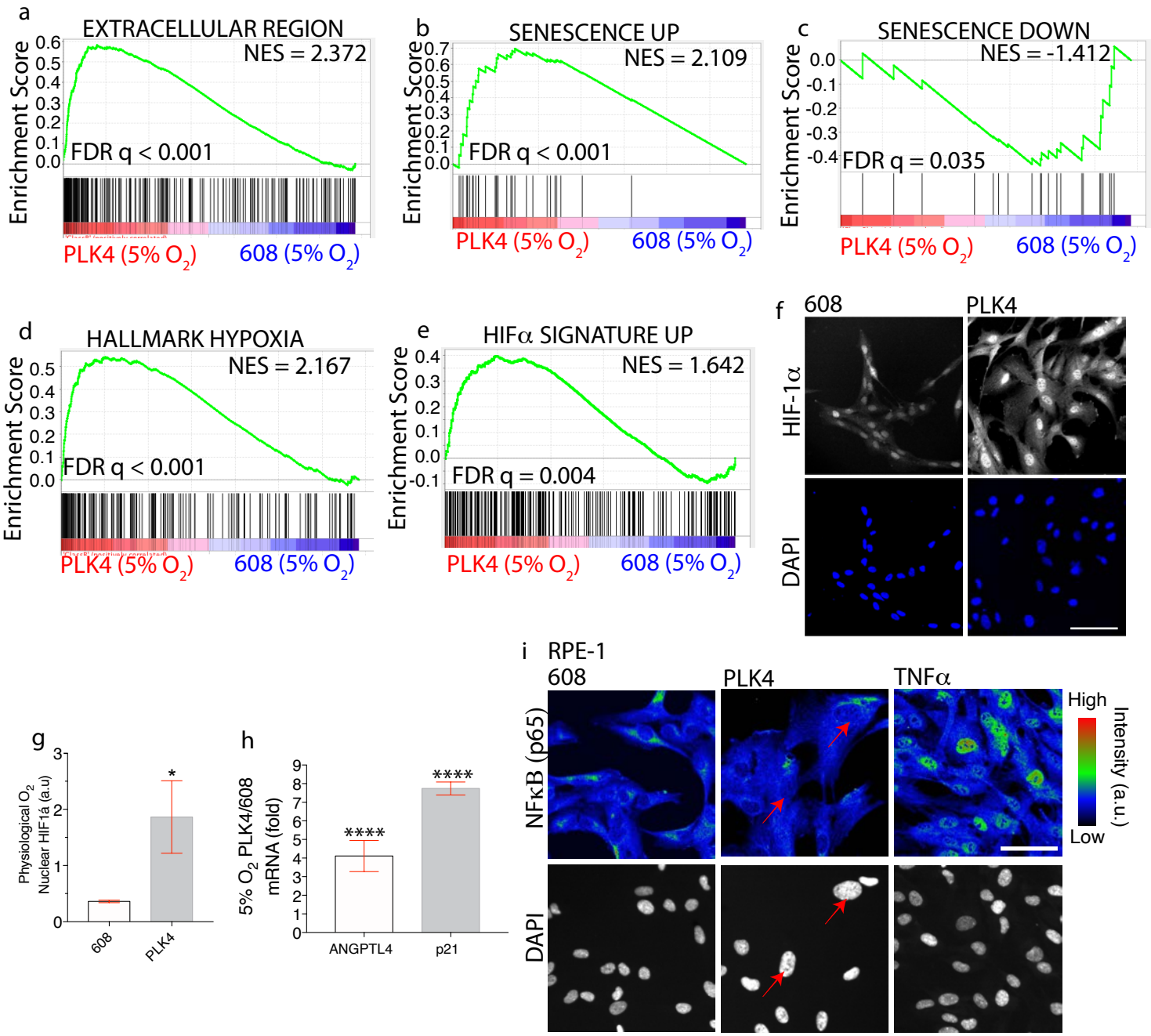
a
EXTRACELLULAR REGION
NES = 2.372
FDR q < 0.001
Enrichment Score
PLK4 (5% O2)
608 (5% O2)
b
SENESCENCE UP
NES = 2.109
FDR q < 0.001
c
SENESCENCE DOWN
NES = -1.412
FDR q = 0.035
d
HALLMARK HYPOXIA
NES = 2.167
FDR q < 0.001
e
HIFα SIGNATURE UP
NES = 1.642
FDR q = 0.004
f
608
PLK4
HIF-1α
DAPI
g
Physiological O2 Nuclear HIF1á (a.u)
608
PLK4
h
5% O2 PLK4/608 mRNA (fold)
ANGPTL4
p21
i
RPE-1
608
PLK4
TNFα
NFκB (p65)
DAPI
High
Low
Intensity (a.u.)

Figure S4

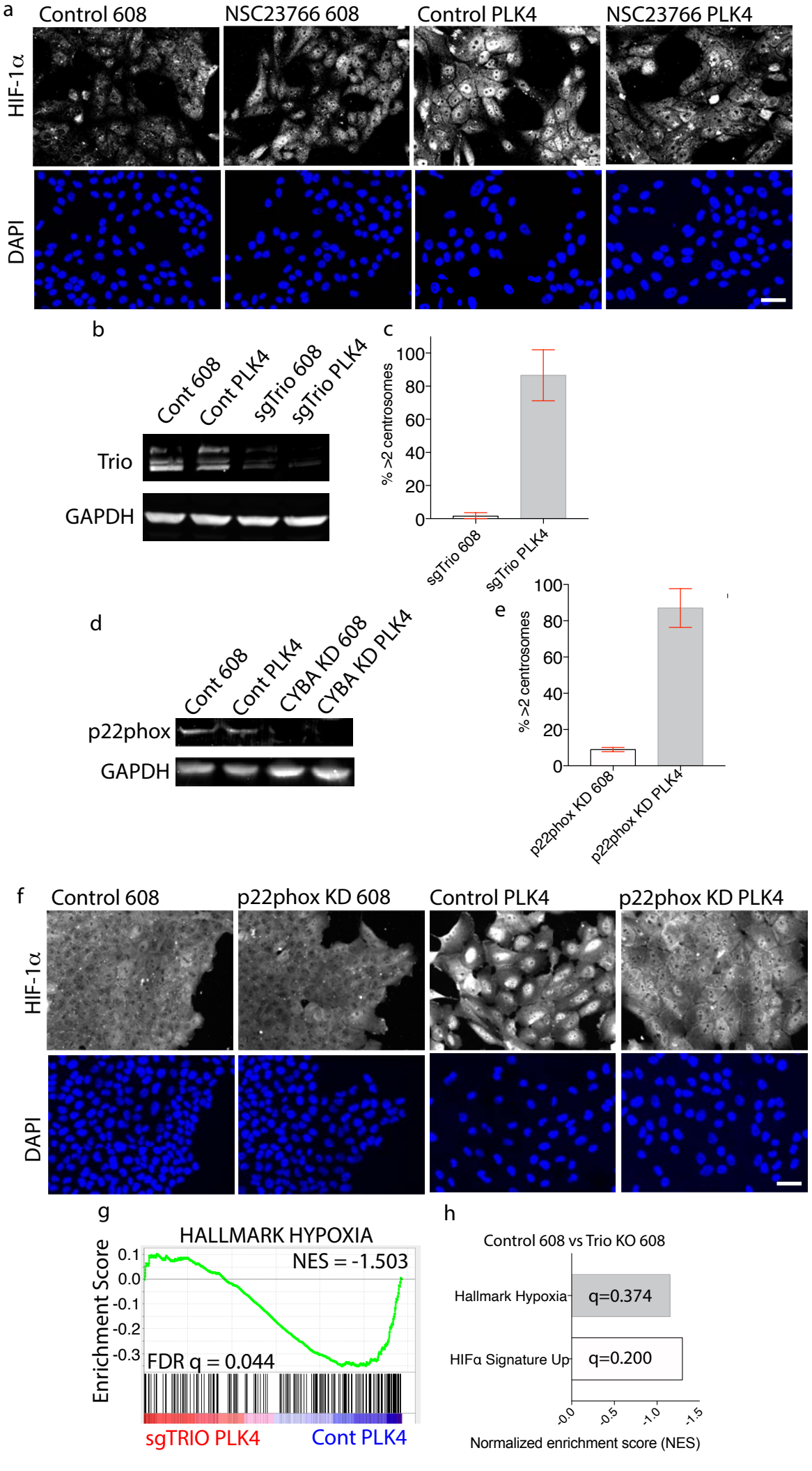
a
Control 608
NSC23766 608
Control PLK4
NSC23766 PLK4
HIF-1α
DAPI
b
Cont 608
Cont PLK4
sgTrio 608
sgTrio PLK4
Trio
GAPDH
c
% >2 centrosomes
100
80
60
40
20
0
sgTrio 608
sgTrio PLK4
d
Cont 608
Cont PLK4
CYBA KD 608
CYBA KD PLK4
p22phox
GAPDH
e
% >2 centrosomes
100
80
60
40
20
0
p22phox KD 608
p22phox KD PLK4
f
Control 608
p22phox KD 608
Control PLK4
p22phox KD PLK4
HIF-1α
DAPI
g
HALLMARK HYPOXIA
Enrichment Score
0.1
0.0
-0.1
-0.2
-0.3
NES = -1.503
FDR q = 0.044
sgTRIO PLK4
Cont PLK4
h
Control 608 vs Trio KO 608
Hallmark Hypoxia
q=0.374
HIFα Signature Up
q=0.200
-0.0
-0.5
-1.0
-1.5
Normalized enrichment score (NES)

Figure S5

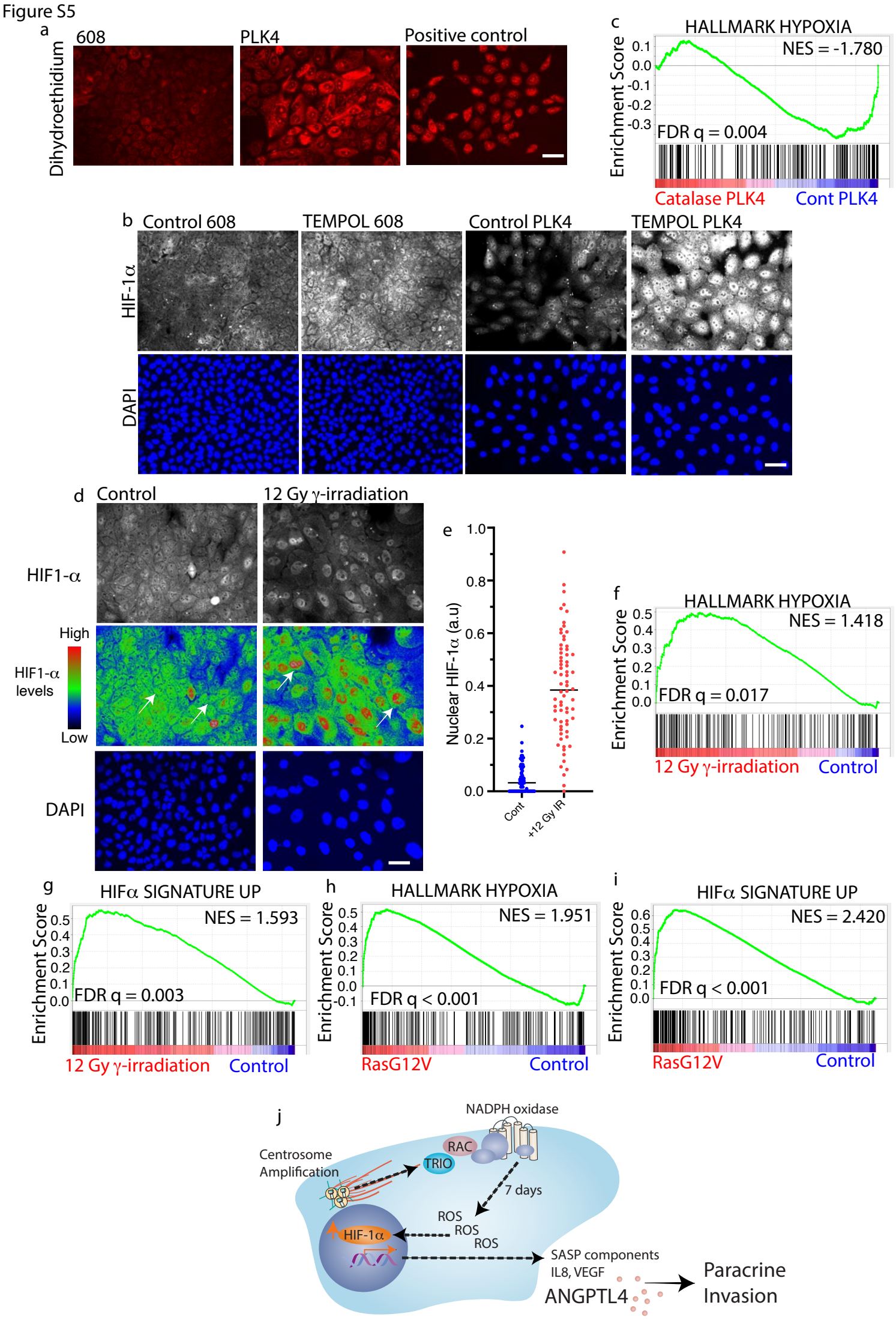
a
608
PLK4
Positive control
Dihydroethidium
c
HALLMARK HYPOXIA
NES = -1.780
FDR q = 0.004
Enrichment Score
Catalase PLK4
Cont PLK4
b
Control 608
TEMPOL 608
Control PLK4
TEMPOL PLK4
HIF-1α
DAPI
d
Control
12 Gy γ-irradiation
HIF1-α
High
HIF1-α levels
Low
DAPI
e
Nuclear HIF-1α (a.u)
Cont
+12 Gy IR
f
HALLMARK HYPOXIA
NES = 1.418
FDR q = 0.017
Enrichment Score
12 Gy γ-irradiation
Control
g
HIFα SIGNATURE UP
NES = 1.593
FDR q = 0.003
Enrichment Score
12 Gy γ-irradiation
Control
h
HALLMARK HYPOXIA
NES = 1.951
FDR q < 0.001
Enrichment Score
RasG12V
Control
i
HIFα SIGNATURE UP
NES = 2.420
FDR q < 0.001
Enrichment Score
RasG12V
Control
j
NADPH oxidase
RAC
TRIO
Centrosome Amplification
7 days
ROS
ROS
ROS
HIF-1α
SASP components
IL8, VEGF
ANGPTL4
Paracrine
Invasion